THESIS FOR THE DEGREE OF LICENTIATE OF ENGINEERING

Tailoring Cellulose Nano- and Microstructures Through Chemical Functionalization and Alignment

JELKA FELDHUSEN

Department of Chemistry and Chemical Engineering

CHALMERS UNIVERSITY OF TECHNOLOGY

Gothenburg, Sweden 2025

Tailoring Cellulose Nano- and Microstructures Through Chemical Functionalization and Alignment

JELKA FELDHUSEN

Technical report no 2025:05

Department of Chemistry and Chemical Engineering
Chalmers University of Technology
SE-412 96 Gothenburg
Sweden
Telephone + 46 (0)31-772 1000

Chalmers Digital Printing Service
Gothenburg, Sweden 2025

Tailoring Cellulose Nano- and Microstructures Through Chemical Functionalization and Alignment

Jelka Feldhusen

Department of Chemistry and Chemical Engineering
CHALMERS UNIVERSITY OF TECHNOLOGY

ABSTRACT

Cellulose, a major structural component of plant cell walls, is a renewable biopolymer known for its mechanical strength and chemical versatility. Traditionally used in the paper and textile industries, it is now drawing increasing attention for applications in emerging fields such as bioplastics, pharmaceuticals, optics, and nanotechnology. This thesis aims to summarize research on the chemical modification of both cellulose fibers and cellulose nanocrystals (CNCs), highlighting how tailored modifications can produce materials with distinct properties and diverse applications.

The modification of softwood based bleached kraft pulp (BKP) was made through the esterification of the hydroxyl groups found on the cellulose fibers using itaconic anhydride. Two methods were explored, mechanical kneading and gas-phase reactions, both gaining BKP-itaconate. The fibers were characterized by a variety of techniques, including Fourier transformed infrared spectroscopy (FTIR), nuclear magnetic resonance spectroscopy (NMR), titrations, powder X-ray diffraction (PXRD) and water absorption. *Manuscript I* explores fiber modification relative to chemical composition but also fiber confirmation and material properties.

CNCs were studied in relation to the counterions and conjugation of azetidinium salts (Az-salts) to the sulfate groups. *Paper II* investigated the influence of different counter ions and sample preparation, i.e. sonication and drying temperature, on the CNCs alignment in films, visualizing their chiral nematic structures with polarized optical microscopy (POM) and UV-Vis. *Paper III* investigated the effects of Az-salts, the effective introduction of alkyl chains to the CNC surfaces, in relation to the rheological properties of the CNC suspensions. Additional work conducted at the B23-Beamline at Diamon Light source (UK) is presented, where Mueller Matrix Polarimetry (MMP) was used to understand the structuring and aggregation of CNCs in films depending on different additives.

Keywords:

Fiber modification, Itaconic acid, Fiber structure, Nanocellulose, Films, Physicochemical properties, Alignment, Azetidinium salts, Mueller Matrix Polarimetry

List of Publications

The thesis is a summary of the following papers.

Manuscript I:

Esterification of Bleached Kraft Pulp with Itaconic Anhydride for Functional Pulp.
Jelka Feldhusen, Kent Malmgren, Tomas Larsson, Gunnar Westman
Manuscript, to be submitted, *Cellulose*

Paper II:

Bendable Transparent Films from Cellulose Nanocrystals–Study of Surface and Microstructure-Property Relationship
Hannah Tideland, Jelka Feldhusen, Amit Kumar Sonker, and Gunnar Westman *Carbohydrate Polymer Technologies and Applications* 2023, *6*, 100367, DOI:10.1016/j.carpta.2023.100367.

Paper III:

Isotropic Gels of Cellulose Nanocrystals Grafted with Dialkyl Groups: Influence of Surface Group Topology from Nonlinear Oscillatory Shear
Sylwia Wojno, Amit Kumar Sonker, Jelka Feldhusen, Gunnar Westman, and Roland Kádár *Langmuir* 2023 *39* (18), 6433-6446, DOI: 10.1021/acs.langmuir.3c00210

Contribution report:

Manuscript I: First author – Conceptualization, planning, design, and experimental work. Analyzing data and writing the manuscript.

Paper II: Second author. Contributed to experimental conceptualization, planning, and design. Analysis of data and contribution to writing.

Paper III: Third author. Performed experimental work and analysis of the results. Contributed to data analysis and writing of the manuscript.

Work related to the thesis has been presented at the following conferences:

Cellulose conference
Karlstad, Sweden 2024 (oral presentation, Manuscript I)

Treesearch Progress
Norrköping, Sweden 2024 (oral presentation, Manuscript I)

EPNOE Junior
Vienna, Austria 2024 (poster presentation, Manuscript I)

ACS Spring
New Orleans, USA 2023 (oral presentation, Manuscript I)

EPNOE
Graz, Austria 2023 (poster presentation, Paper II and III)

Tetrahedron
Gothenburg, Sweden 2023 (poster presentation, Paper III)

List of Abbreviations

BKP – Bleached kraft pulp

BKP-Itaconate – Esterified BKP

$\mathrm{BKP}_{\mathrm{LE}}$ – Liquid exchanged BKP

$\mathrm{BKP}_{\mathrm{ND}}$ – Never-Dried BKP

CD – Circular dichroism

CNC – Nanocrystalline Cellulose/Cellulose nanocrystal

CNF – Cellulose nanofibril/Cellulose nanofiber

ECH – Epichlorohydrin

FTIR – Fourier-transformed infrared spectroscopy

Gly - Glycerol

H_2IA – Itaconic acid

H_2O - Water

iPrOH – Isopropanol/2-propanol

ITA – Itaconic anhydride

LB – Linear birefringence

LD – Linear dichroism

MCC – Microcrystalline cellulose

meq – milli-equivalence

MMP – Mueller matrix polarimetry

NMIM – N-Methylimidazole

NMR – Nuclear magnetic resonance spectroscopy

polyBRENE - poly(hexadimethrine) bromide

polyDADMAC - poly(diallyldimethylammonium) chloride

PXRD – Powder X-ray diffraction

TBV – Tea bag value

TEOA - Triethanolamine

WRV – Water retention value

Table of Contents

CHAPTER 1
INTRODUCTION

1.1 Background

Advancing toward a more sustainable society requires the development of innovative materials derived from renewable and sustainable resources. Cellulose, widely recognized as the most abundant natural polymer (Aziz, Farid et al. 2022, Tanpichai, Boonmahitthisud et al. 2022), presents significant potential as a fundamental building block for such materials. Owing to its renewability, mechanical strength, and chemical tunability, cellulose serves as a versatile platform for the design of high-performance alternatives across various application areas.

Cellulose consists of glucose-monomers, which are connected through beta-1,4-glucosidic linkages between the anhydroglucose (AGU) repeating units (O'Sullivan 1997, Kadla and Gilbert 2000). On each of these monomers, three hydroxyl groups are present on the C2, C3, and C6 carbon, Figure 1, which are useful when wanting to perform chemical modification on the cellulose.

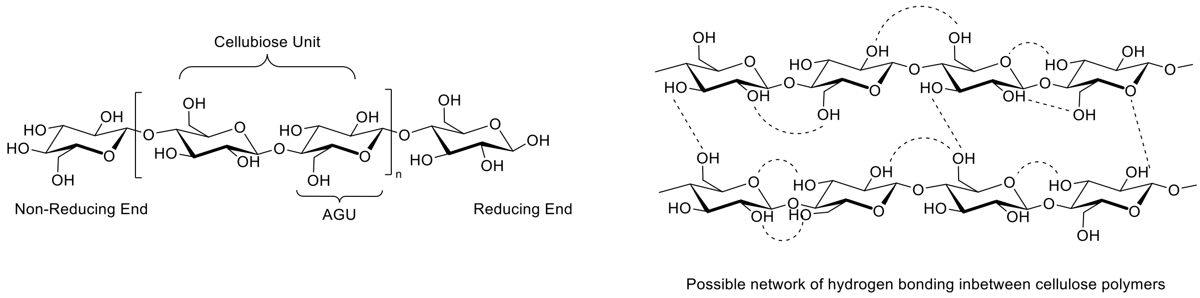

Figure 1. Left: Presentation of the structure of cellulose. The number of cellobiose units, n, is dependent on the size of the source, shape and treatment of the cellulose fibers. Right: Inter- and intramolecular interactions of hydrogen bonds.

Softwood based bleached kraft pulp, BKP, used in parts of this thesis, consists largely of cellulose and is today utilized to produce paper and paperboard. Through mechanical and chemical modifications, its surface and bulk properties may be altered, creating products which are tailored towards its desired use. New developments in the cellulose field have created broader possibilities to expand their applications, for example as a plastic alternative or complement. Cellulose based fibers show great tensile strength, whilst remaining flexible, useful when wanting to replace some fossil-based products. In combination with chemical modifications and additives, for example crosslinking for greater wet strength and hydrophobization agents as a barrier, the application of cellulose-based materials becomes even wider, as in single-use takeaway boxes, or similar. Comparably, nanocellulose and composites thereof may be used where the material required transparency, as in wrappings, optical materials, or similar.

Part of this work presents the chemical modifications of pulp by introducing carboxylic acid functionalities using the anhydride of itaconic acid (H_2IA), a bio-based and non-toxic carboxylic acid. The modification is achieved through the esterification of itaconic anhydride (ITA) with the hydroxyl groups on cellulose.

The ring-opening of the anhydride, either at the C1 or C4 position of ITA, effectively decorated the fibers with itaconic groups, as seen in Figure 2.

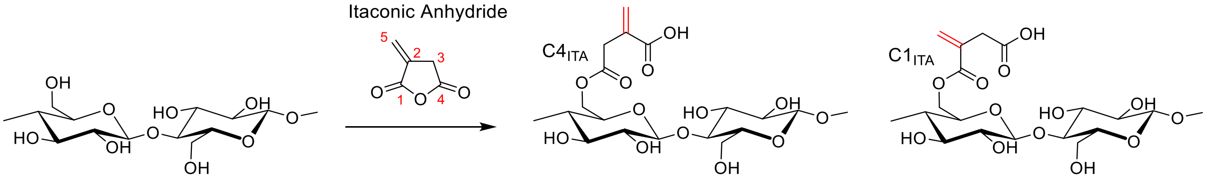

Figure 2. Esterification of cellulose with itaconic anhydride (ITA) through the C1 or C4 carbon.

The esterification of BKP was performed on never-dried and liquid-exchanged dry pulp (BKP_{ND} and BKP_{LE}, respectively) with low cost and low energy methods, namely through high-consistency mixing and gas-phase reactions.

In parallel to the modification of fibers, the modification and aggregation of sulfonated nanocrystalline cellulose (CNC) was studied. As cellulose fibers include both ordered and less ordered domains, CNC was thought of as a model compound to understand the relation between chemical modification and crystallinity, surface-availability, and conformation. This has, as of yet, never been studies before, but grafting of alkyl groups on CNCs have been shown to have an effect on the CNC structure, likely also occurring during the chemical modification of pulp. The modification of CNCs were made using azetidinium salts (Az-salts) to graft alkyl chains on the CNC surfaces or through the addition of counter ions, such as Na^+ or amines, to understand their effect on intramolecular interactions and arrangement (Figure 3). The properties of the CNCs with and without chemical modification by themselves were also studied exploring their optical properties, such as their birefringence.

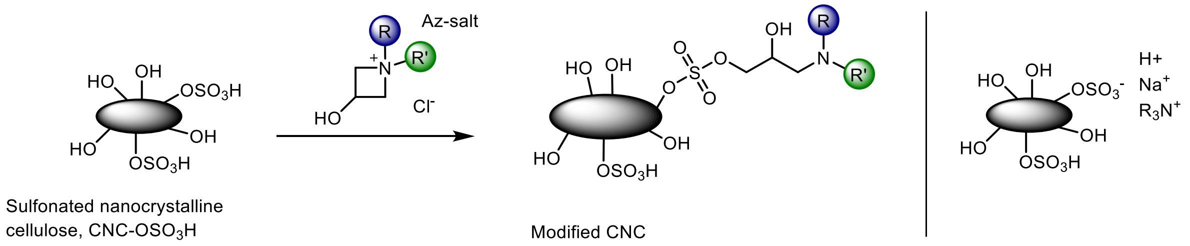

Figure 3. Illustration of the modification of sulfonated CNC with Az-salts (left) or different counterions (right).

1.2 Aim

This thesis aims to combine knowledge from two fields of cellulose research, fiber and CNC modification, to generate a broader picture and an increased understanding of a complex system. As stated, cellulose fibers found in pulp contain more ordered, crystalline domains alongside amorphous regions. To fully understand the ordering and structure of cellulose fibers and hence create a better foundation for selective modification and the formation of advanced materials, CNC studies were conducted in parallel to the fiber modification, and conclusions drawn between the fields.

The detailed aims of this thesis are to:

I. Use itaconic acid or anhydride for the modification of bleached kraft pulp to gain functionalized fibers, useful in water absorption, barrier or packaging applications.
II. Understand the mechanism of the esterification of BKP using itaconic anhydride based on different reactions, pulp composition, crystallinity, and accessibility.
III. Explore the structural effects of crystallinity and water interactions with cellulose fibers using CNCs as model compound.
IV. Gaining insight into the role of alignment and crystallinity of pristine and modified CNC, for parallels to fiber modification and the fabrication of optically active material

CHAPTER 2
FIBERS

Cellulose fibers, originating from both lignocellulose (a matrix of cellulose, hemicellulose, and lignin) and cotton, are used in everything from paper and packaging to construction, food, and medical applications. The extraction process and the chemical and physical manipulation of the fiber structure all influence the properties of the cellulose fibers creating a variety of different products.

2.1 Source, Structure, and Reactivity

Throughout this thesis and its fiber project, softwood based bleached kraft pulp (BKP) was used. Bleached kraft pulp (BKP) is produced through the Kraft process, which involves cooking softwood with a solution of hydroxide and hydrosulfide ions, followed by bleaching with chlorine dioxide and subsequent washing. Softwood fibers, which are typically longer than hardwood fibers, form paper with great tensile and mechanical properties. The cooking and bleaching stages also remove the majority of lignin and some hemicelluloses present in softwood, resulting in high-quality pulp, suitable for chemical modification.

The structure of cellulose fibers is hierarchical, as each fiber consists of fibrils, which themselves consist of cellulose nanofibers and eventually individual cellulose polymers (Matveev, Vasilevsky et al.), presented in Figure 4. Each cell consists of several layers with different molecular composition (presence of hemicelluloses or lignin) and supramolecular structures such as the direction of the cellulose polymers. The interaction of hemicellulose with cellulose and lignin is complex since the hemicellulose in the pulp are heterogenous in their carbohydrate arrangement leading to consequential effects on the fibers structure. The primary structure of the carbohydrate sequence of the hemicellulose chain, that is the type of saccharide, leads to the secondary structure, with either a linear or branched spatial arrangement of oligosaccharide segments. This results in a tertiary, the three-dimensional, structure of the hemicellulose affecting the quaternary structure on how the three-dimensional structures interact with the cellulose and lignin in the individual fiber and pulp. (Kabel, van den Borne et al. 2007, Eronen, Österberg et al. 2011)

It has been shown that the presence of hemicellulose influences the material response of cellulose fibers, that is reducing the effect of so-called hornification linked to irreversible changes in the fiber structure, possibly because of the branching of the supramolecular structure thereby hindering the pores in the fiber wall from closing. (Spinu, Dos Santos et al. 2011) Furter, some studies have been conducted on the addition of xylan-based hemicelluloses to pulp, in attempts to reduce this hornification (Köhnke 2010). Additionally, the presence of the lignin, although small, may also influence the structure of the pulp and cellulose fibers.

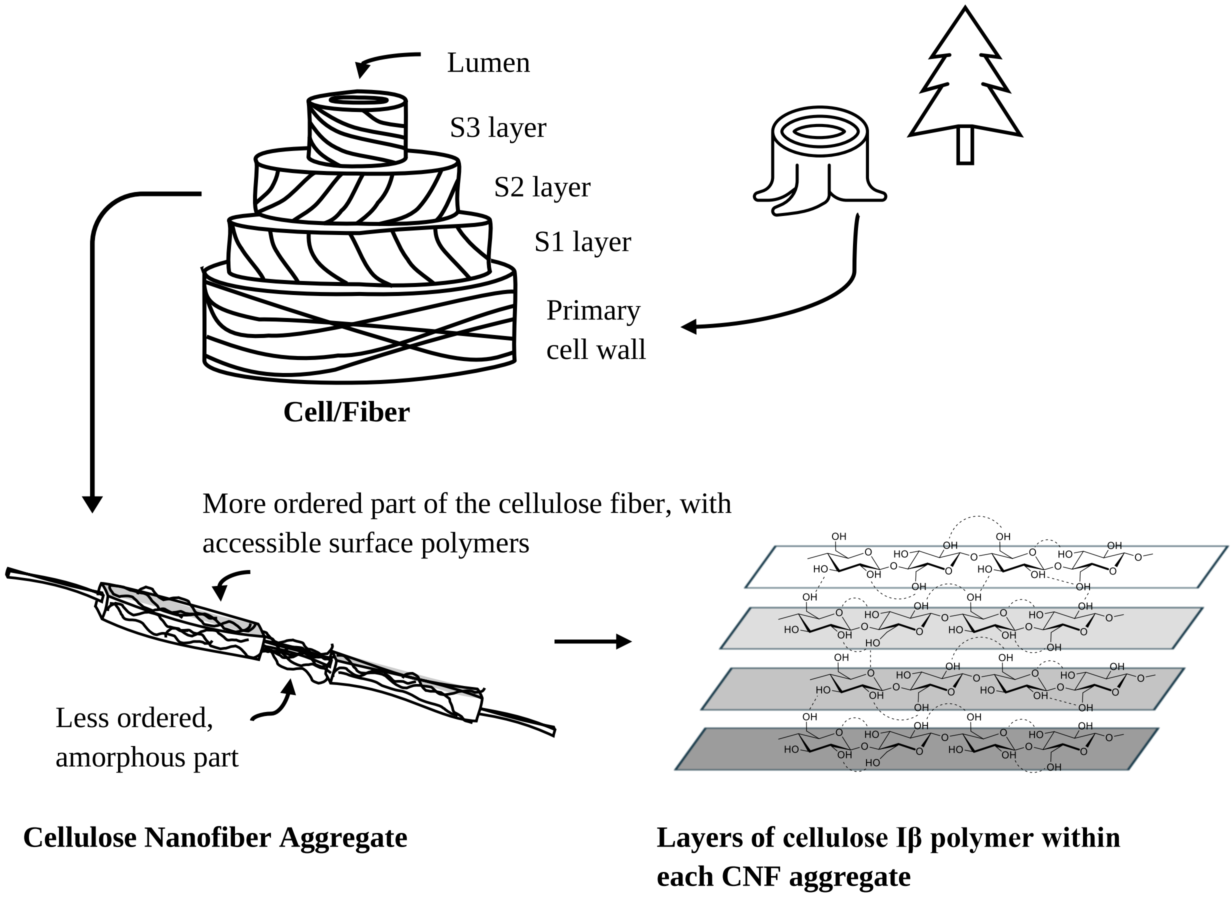

Cell/Fiber

Cellulose Nanofiber Aggregate

Layers of cellulose Iβ polymer within each CNF aggregate

Figure 4. The hierarchical structure of wood and fibers alongside cell-wall composition, from tree to individual cellulose layers. The cell-wall is divided into several layers, having a varying cellulose content and polymer direction (indicated with lines). The S2 layer being the thickest contains the most nanofiber aggregates which themselves consist of more and less ordered regions. Within each of these, the polymers are stacked into layers being held together by hydrogen bonding. Noteworthy is that the more ordered regions still present amorphous surface polymers, available for modification and interaction with their environment. Adapted from (Ek, Gellerstedt et al. 2007, Matveev, Vasilevsky et al. 2022)

Alongside composition, the water content also strongly affects the fibers' states through swelling, opening of the structure, and hornification, as stated, a tightening or shrinkage of the fiber network through hydrogen bond rearrangements (Hribernik, Stana Kleinschek et al. 2016) and irreversible pore closure (Stone and Scallan 1968, Spinu, Dos Santos et al. 2011).

Swelling refers to the process of emerging fibers in water (or other liquids). In water, the swelling is a rather fast process, starting with the wetting and saturation of the fiber surface, before penetrating deeper into the interfibrillar spaces, capillaries, and lumen of the cell wall, effectively disrupting the hydrogen bonding between the individual cellulose fibrils within the fiber and gaining an increase in volume. (Botková, Suty et al. 2013) Pre-swelling or swelling with sodium hydroxide (NaOH) results in a more open pulp structure, as sodium ions form layers between the cellulose fibrils, increasing accessibility to both the internal structure and the hydroxyl groups. The swelling achieved with sodium hydroxide and other alkaline solutions is directly influenced by the base concentration, the hydrated radius of the alkali metal ion, and the temperature at which the swelling is conducted. (Hribernik, Stana Kleinschek et al. 2016). At too high concentrations of swelling agents, solvents, or reagents conducted at the wrong temperatures may, instead of swelling, lead to the depolymerization of cellulose thereby resulting in shorter fiber fragments and, in some cases, undesired mechanical properties. It should also be kept in mind that different cellulose sources correspond differently to different swelling agents, because of their inherent differences in structure and type of cellulose. An increase in charge density of the fibers further influences their swelling (Sjöstedt, Wohlert et al. 2015), due to their effect on the cellulose structure, which is especially important for chemically modified fibers and the application thereof. Likewise, the size of the cellulose fibers also strongly influences the degree of swelling, as shorter fibers have a larger surface-to-volume ratio. As an example, cotton, often seen as a model substrate for cellulose, has been shown to swell well in sodium hydroxide, DMSO, and acetonitrile (El Seoud, Fidale et al. 2008). Although swelling seems favorable for derivatizations of cellulose, it may in some cases hinder derivatization, depending on the type of chemical reaction.

For some of the chemical modifications a liquid exchange (LE) of the pulp was performed, that is, exchanging the water present in the pulp for another liquid/solvent. After first washing with ethanol to replace the water, acetonitrile is used to exchange to an aprotic solvent. The pulp is thereafter dried at a low temperature, mostly preventing the effect of hornification, and keeping a “fluffier” pulp with higher chemical reactivity due to lesser intramolecular bonding. It should be noted that the type of drying, at room temperature, at elevated temperatures, through vacuum, of freeze drying also all influences the chemical reactivity and degree of hornification of the fibers. (Spinu, Dos Santos et al. 2011) In this project acetonitrile was used due to its known property to swell fibers, its availability, cost, and green solvent profile. Similarly, acetone is used in the derivatization of fibers due to its comparatively low toxicity (Alder, Hayler et al. 2016) and availability. In this project alcohols are overruled due to their protic nature, thereby competing with the hydroxyl groups found on the cellulose fibers.

As stated, the effects of hornification are just as important as the swelling of fibers. In the paper industry, hornification is sometimes used as an advantage in some products, for example in barrier materials as it, together with some chemical additives, gains higher wet strength or water resistance. In other cases, hornification is seen as more of a problem, especially in absorbing materials.

The changes in the fiber structure, i.e. through hornification, may be visualized using so called water retention values (WRV), as drying and rewetting of the fibers changes their structure. In addition to WRV values, Powder X-ray diffraction (PXRD) and solid-state nuclear magnetic resonance (NMR) are often used to study the change in crystallinity resulting from chemical modification, hornification, or swelling.

PXRD is a bulk method used to assess the crystalline domains found in fibers and is useful for assessing the average crystallite size which can elucidate the effects of chemical modification on fiber degradation. For native lignocellulose, rich in cellulose Iβ (Nishiyama, Sugiyama et al. 2003), the (200) plane can be used to assess the length of L_{200}, the average crystalline width. Other planes, such as the (110) or (1-10) and (004), may also have been found in the structure as illustrated in Figure 5. The crystal structure makes cellulose crystals anisotropic and consequently reflect and scatter light differently depending on the light direction. This property is useful when assessing materials properties, not only useful for cellulose fibers but also for CNCs.

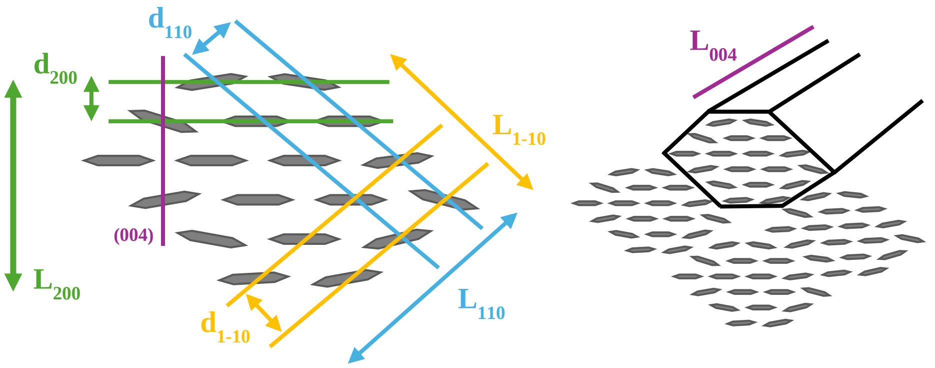

Cross-section of the nano/micro fibril, cellulose Iβ - Monoclinic

Fiber aggregate from four nanofibers

Figure 5. Left: The crystalline structure of cellulose Iβ. Adapted from Paajanen (2022), Han (2023), and Åhl (2025). (Paajanen, Zitting et al. 2022, Han, Chen et al. 2023, Åhl, Ruiz-Caldas et al. 2025). Left: Illustration of one nanofibril, with assigned crystal planes. The propagation of the cellulose chain extends into the paper. Right: Illustration of fiber aggregate, here illustrated from four nanofibers, illustrating the assembly of individual fibrils into larger aggregates.

Solid-state NMR is a collective name for different NMR techniques performed in the solid state of materials. For cellulose, CP/MAS ^{13}C-NMR is most used, sometimes in complement with the newer and more powerful DP-NMR, specifically useful for the surface characterization of fibers. Here, CP/MAS ^{13}C NMR was utilized to investigate the fiber ultrastructure and the potential site of modification.

As described by Hult et al. (2002), Virtanen et al. (2008), and others, the C4 region in the NMR spectrum is generally of interest for cellulose samples, specifically between 80-92 ppm, and is the sum of different signal contributions. (Larsson, Wickholm et al. 1997, Larsson, Hult El Fau - Wickholm et al. 1999, Hult, Larsson et al. 2002, Virtanen, Liisa Maunu et al. 2008) Crystalline cellulose I allomorphs, cellulose Iα (89.5 ppm), I(α+β) (88.8 ppm), and Iβ (87.9 ppm) all contribute to the signal, with some contributions from non-crystalline cellulose forms, namely para-crystalline cellulose (88.7 ppm), accessible fibril surfaces (84.3 ppm and 83.3 ppm), and inaccessible fibril surfaces (83.8 ppm) (Wickholm, Larsson et al. 1998, Hult, Larsson et al. 2002). Hemicellulose, if present, also contributes to some extent with signals at 81.7 ppm or two separate signals at 81.9 ppm and 81.2 ppm. (Larsson, Wickholm et al. 1997, Hult, Larsson et al. 2002)

PXRD gives the crystalline-uniform organized part of the fibril, whereas ssNMR gives information on all the cellulose polymers in the fibril. Thus, these two techniques complement each other, but they are not expected to give the same results.

2.2 Chemical Modification in General

Generally, chemical modifications are made at the C6 carbon of cellulose, containing the primary hydroxyl group as they are most accessible (Figure 6). The different conformations of the C6-hydroxyl group (trans-gauche, tg, or gauche-trans, gt) allow the C6-OH to be flexible and thereby available for chemical modification. The orientation of the C6-OH is also responsible for the crystalline structure of cellulose, being predominantly tg in anti-parallel cellulose I, whilst being predominantly gt in the parallel cellulose II (Wohlert, Benselfelt et al. 2022).

Utilizing the C6-hydroxyl group, many types of modifications can be made, non the least esterification (in this project) or ether-formation as in carboxymethylated cellulose (CMC) found in toothpaste, as a food additive, stabilizer, or coating (Nouryon 2025).

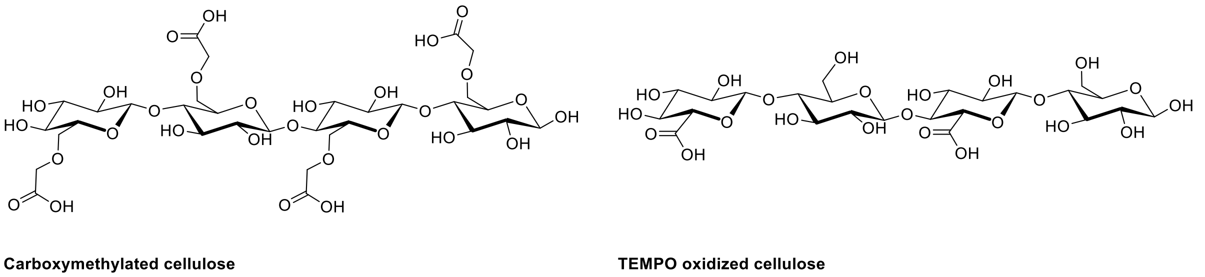

Figure 6. Common chemical modification of cellulose. Left: Carboxymethylated. Right: TEMPO oxidized cellulose. Note that on CMC all the primary hydroxyl groups are functionalized, due cellulose being dissolved during the modification process, whereas for TEMPO oxidized cellulose, the carboxylic acid has only been drawn on one side of the cellulose polymer, as this reaction only occur on the microfibril surface.

The degree of modification, also called substitution (DS) value, describes the number of hydroxyl groups substituted at each AGU as an average per mass of fiber. As each AGU contains 3 OH groups, the theoretical maximum value is 3, although never achieved experimentally. DS values of 0.1-0.3 are seen as high for intact fibers, whilst the modification of MCC, as for CMC, can gain values close to 2.7-2.8.

Other types of modification include cross-linking cellulose fibers for higher wet strength, increasing the mechanical properties both in a wet and dry state. Crosslinking can be made with a variety of different compounds. In industry, mostly resins such as urea-formaldehyde, melamine-formaldehyde, and polyamide-epichlorohydrin (PAE)-based compounds are used, Figure 7. Others may be alkyl ketene dimer or alkenyl succinic anhydride. (Francolini, Galantini et al. 2023)

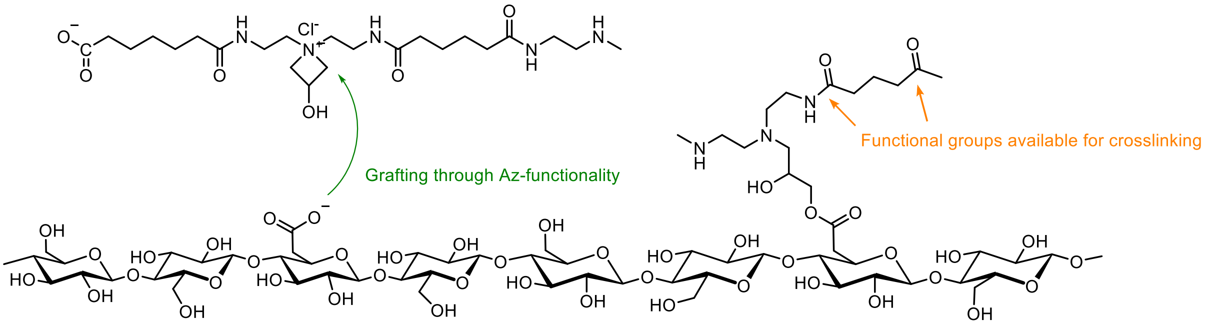

Figure 7. Crosslinking of cellulose fibers using PAE-based compounds through Az-functionality and other functional groups.

2.3 The Use of Itaconic Acid and Itaconic Anhydride on Pulp

Itaconic acid (H_2IA) is a dicarboxylic acid, containing an unsaturation in the middle of the molecule. It is, amongst other pathways, produced by microorganisms (Teleky and Vodnar 2019, Kerssemakers, Domenech et al. 2020), is non-toxic and is seen as a potential future platform chemical (Werpy and Petersen 2004). Its anhydride, itaconic anhydride (ITA), is produced upon heating of the acid, whereas the acid can be re-formed through hydrolysis of the anhydride in water. Further, it has been shown that itaconic acid can isomerize into mesaconic or citraconic acid at high temperatures, >150 °C (Figure 8).

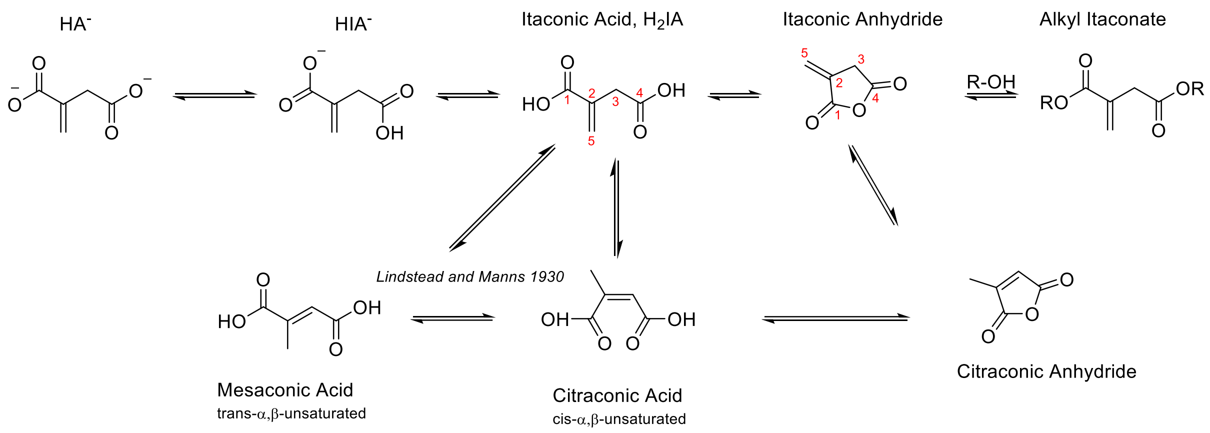

Figure 8. Correlations between itaconic acid and anhydride, including isomer structures.

H_2IA is mostly used in polymer chemistry as a monomer, creating polymers containing carboxyl groups. It has been reported that the polymerization of H_2IA is successful in 0.5 M HCl at 50 °C, gaining poly(itaconic acid) (PIA) (Stawski and Polowinski 2005), whilst others state that the neutralization of the itaconic acid results in polymers. Several papers have been published on the use of H_2IA on biopolymers such as starch (Soto, Urdaneta et al. 2016), chitosan (Sirvio, Kantola et al. 2021) and chitin (Mostafa, Naguib et al. 2005).

H_2IA has a lower reactivity for esterification reaction compared to the ring closed anhydride, ITA. For the ITA, esterification occurs, either through the ring opening at the $C1_{ITA}$ or $C4_{ITA}$ position, reacting with the C6 hydroxyl group of cellulose. Due to the two different carbons, and the isomerization of the itaconic-functionality (Figure 8), up to six different outcomes are theoretically expected, as described in Figure 9.

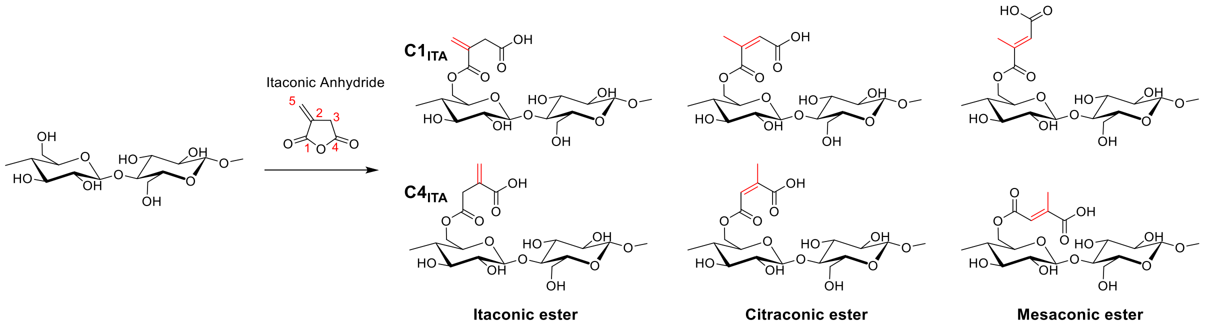

Figure 9. Conjugation of ITA to BKP, with possible isomers, specifically different localization of the C=C bond.

During the chemical modification, different sites of the fiber are decorated, depending on the fiber network accessibility, altered by swelling, hornification or presence of branched or charged groups. This leads to a variety of charges being present which may be separated into the following categories.

1. Fully accessible charges – located on the outer surface of the fibers, readily available for interaction with large molecules, other reagents, or polyelectrolytes.
2. Partially accessible charges – found within the fiber wall or fibrillar network; they may be accessible to smaller polymers and reagents.
3. Buried or inaccessible charges – located deep within the fiber structure, only measurable and accessible by small ions.

CHAPTER 3
NANOCRYSTALLINE CELLULOSE, CNC

Nanocrystalline cellulose or cellulose nanocrystals, CNC, are small nano-sized particles from cellulose. Although being to some extent chemically identical with cellulose fibers, they exhibit different properties and may be used for either as model substrate, or in special applications such as electronics, optically active materials, or medical applications.

3.1 Nanocellulose fibers (CNFs) and Nano-crystalline cellulose (CNC)

Both cellulose nanofibers (CNF) and nanocrystalline cellulose (CNC) may be produced from cellulose fibers (Figure 10). Classically, CNFs are produced by the mechanical shearing of TEMPO-oxidized fibers, that is, fibers with high surface charge. CNFs are seen as a versatile building block for materials, including gels and advanced functional materials. They contain both more and less ordered regions, being 3-100 nm wide and up to 100 µm long. Important is the ratio, which according to ISO should be > 10. (Fernandes, Cruz-Lopes et al. 2023) CNFs have also reached the commercial market, with a production of 500 metric tons per year by Nippon Paper in their facility in Ishinomaki, Japan (Matsuoka 2023, Group 2025).

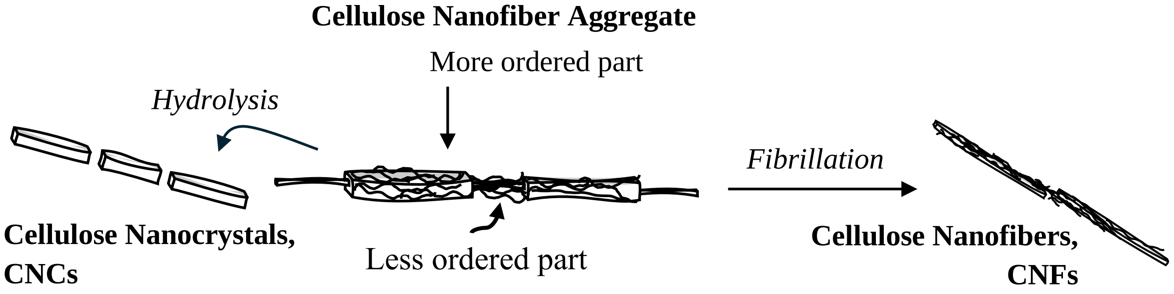

Figure 10. Illustration of CNF and CNC, both made from cellulose but treated differently, adapted from (Fernandes, Cruz-Lopes et al. 2023). In the figure, the CNC and fiber aggregates are displayed as having a rectangular shape, however, this is only an adaptation as their structures are more complex and not definite.

CNCs, as compared to CNFs, only contain highly crystalline regions, having a discrete rice or rod-shaped structure. ISO standards classify CNCs as having a diameter of 3-50 nm and a length between 100 nm to several µm. Depending on the source of cellulose and extraction process, the size and surface chemistry varies of the crystals. (Fernandes, Cruz-Lopes et al. 2023)

CNCs are generally produced through the hydrolysis of amorphous regions found in microcrystalline cellulose (MCC) or pulp fibers. Depending on the acid used, different surface groups are consequently introduced to the CNC surface (Figure 11), giving the suspensions different properties. Using sulfuric acid gains CNC with sulphate half-esters on the cellulose surface, CNC-SO_3H, with suspensions having high colloidal stability. Using phosphorus acid gains phosphorus half-esters, CNC-PO_3H, whilst hydrochloric acid gains “uncharged” CNC with only hydroxyl groups on the surface, CNC-H. (Wang, Tang et al. 2022)

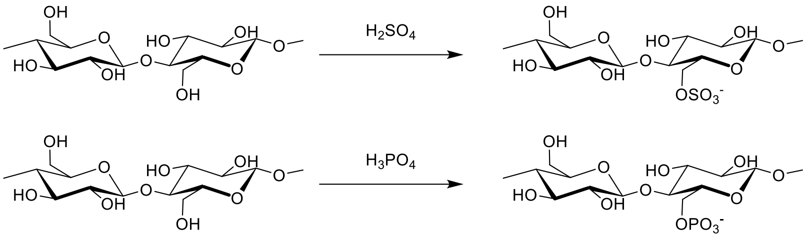

Figure 11. Top: Formation of CNC-OSO3⁻, made from sulfuric acid and microcrystalline cellulose. Bottom: Synthesis of CNC-OPO3⁻ using phosphoric acid.

The exact structure of CNCs is still debated; some say that they are rod-shaped and symmetrical, whilst others say that there is a difference in the number of cellulose polymers in the cross-section, giving it a square or hexagonal shape, affecting its reactivity on the different sides of the CNC crystal. Additionally, the source of cellulose heavily dictates the morphology of the CNCs. (Wang, Tang et al. 2022)

In connection with fiber modification, the CNC-H is the most representative as a model substrate. However, their high uniformity and lack of large surface groups leads to them aggregating into large clusters with a low number of accessible hydroxyl groups thereby yielding low reactivity, making them difficult to chemically modify. Due to this, studies on the more stable CNC-OSO_3H were conducted.

3.2 Optical properties and arrangements/alignment of CNC

CNC behaves as a liquid crystalline phase in water with anisotropy and birefringence, and may, upon drying, arrange in different domains and aggregates, exhibiting different material properties. Some of the most determining variables for the aggregation are the crystal size, charge, and concentration, which also all influence the so-called pitch length (see Figure 13). Crystals obtained from bacterial cellulose, having a ribbon-like structure, have a half-helix pitch of 600–800 nm, while CNC from tunicate has a half-helix pitch of 1.2–1.6 μm. Because of this, their interaction with light is different from one another, although both are CNC.

3.2.1. Definitions

I. Aggregation-states of CNC:

CNCs are either self-assembling or non-self-assembling. Self-assembling refers to a system where the attractive forces out-rule the repulsive ones in the system, for CNC occurring above the critical volume fraction φ^*. Likewise, non-self-assembling suspensions of CNC are isotropic but mostly exist in very dilute systems, with aggregation occurring with higher concentrations, forming an attractive glass phase. At high ionic strengths (highly charged CNCs), the isotropic suspensions form an isotropic gel to an attractive glass state with increased concentration. At low ionic strength, the CNC moves to a more biphasic to liquid crystalline and lastly repulsive glass state with increased concentration, Figure 12. (Wojno 2023)

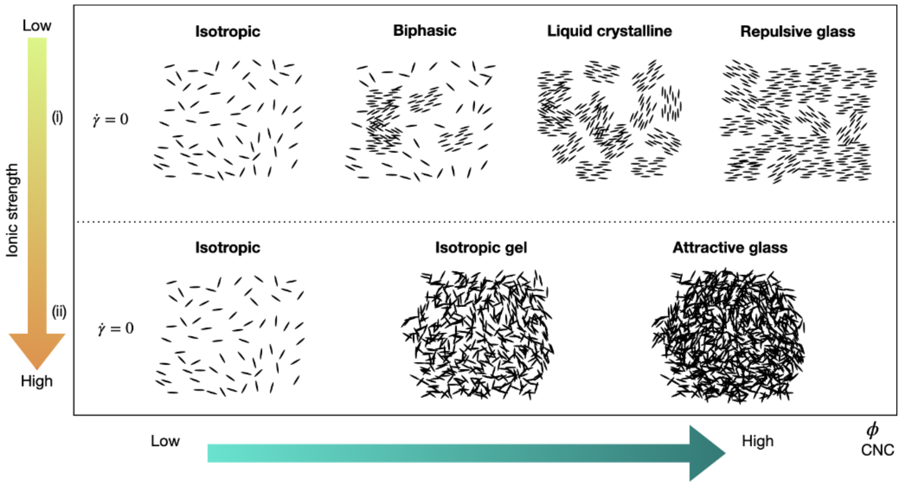

Figure 12. A schematic of different aggregation stages of CNCs, vary with surface charge and concentration. Illustration from Sylwia Wojnos PhD thesis, (Wojno 2023).

II. *Isotropy and Anisotropy:*

An isotropic system is said to have no order, or the same properties in all directions. Anisotropy is the property describing directional dependency, that is, not all orientations are the same, and the sample has direction-dependent properties.

III. *Chiral Nematic and Smectic Phases:*

The nematic phase is the alignment of molecules along one axis. The chiral nematic (cholesteric) phase is a subclass and occurs only in chiral molecules and is the twisted assembly of structures perpendicular to the director. CNCs often exhibit an anticlockwise direction of the twist, as also seen in Paper II. The smectic phases, another subclass to nematic phases, are generally found at lower temperatures compared to the nematic phases and form well-defined layers that may slip over one another. Depending on how the molecules align, different types of smectic phases are observed. Figure 13 illustrates the different nematic phases.

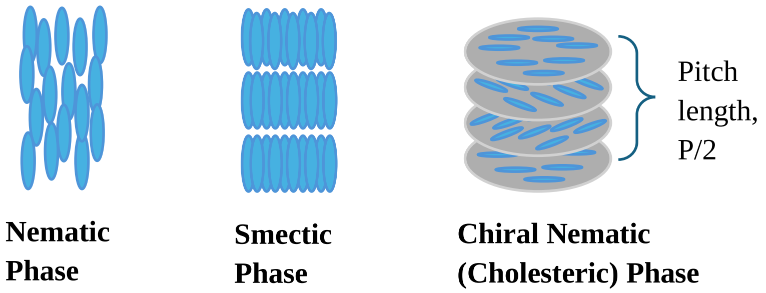

Figure 13. Illustration of the liquid crystal structures: Nematic, Smectic and Chiral Nematic (Cholesteric).

IV. *Pitch-length:*

As mentioned, CNC may arrange into mesophase structures of aggregates in a cholesteric fashion, exhibiting different so-called pitch lengths, Figure 13. The pitch length is defined as the distance between two discs in the chiral nematic phase reaching the same orientation in relation to the director. Additionally, a variation in the pitch length of the crystalline chiral aggregate induces differences in the interactions with light, giving them different colors and properties depending on their aggregation and source. Due to this interaction, they are interesting for applications in the field of optics and sensors.

V. *Birefringence:*

Birefringence, or double refraction, describes the interaction between matter and light, which depends on the propagation direction and polarization of the light. Anisotropic (directionally dependent ordered) matter expresses birefringence, such as arranged CNC films.

VI. *Linear and Circular Dichroism:*

Linear dichroism (LD) is the difference in absorption between linearly polarized light, orthogonal to one another. Generally, anisotropy is required to generate a signal; that is, the molecules are somewhat aligned. The circular dichroism (CD) is the difference in absorption between left and right-circularly polarized light. The CD signal provides details of the dissymmetry in a molecule and can only be detected for three-dimensional structures, like CNC crystals. Figure 14 visualized the formation of linear (left) and circular (right) polarized light. Note that the linear polarized light also can be rotated by 90°. The circular polarized light is either left or right directional about the axis and penetrates the sample as a spiral with a forward direction along the axis.

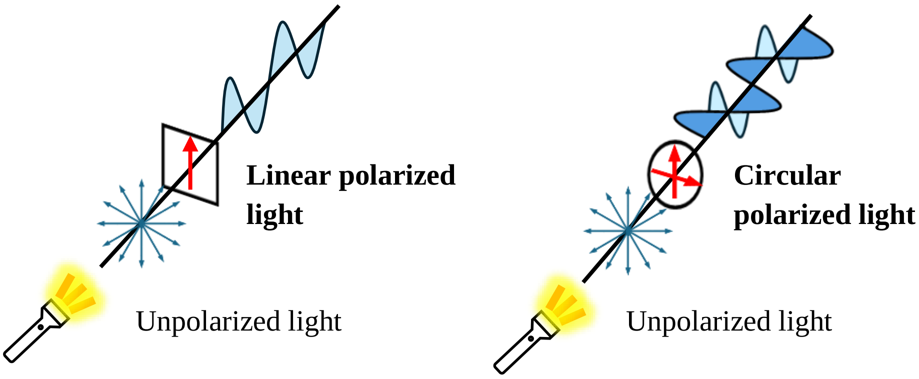

Figure 14. Illustration of linear and polarized light, along one axis.

3.3 Covalent and non-covalent modification and alignment of CNCs

A key challenge in utilizing CNC-OSO_3H is its tendency to self-assemble into ordered structures, which define its optical, mechanical, and structural properties. (Frka-Petesic, Parton et al. 2023) Revol et al. (1994) first reported that CNC-OSO_3H suspensions spontaneously separate into ordered and disordered phases, with the ordered phase forming chiral nematic structures. (Revol, Godbout et al. 1994, Revol, Godbout et al. 1998) Their pioneering work showed that CNC undergoes an isotropic-to-chiral liquid-crystalline phase transition above a critical concentration, leading to photonic properties upon drying. (Revol, Bradford et al. 1992, Chu 2024).

Inorganic ions such as K^+ and Na^+ may suppress the anisotropic phase formation due to increasing the critical concentration of the suspension to form strictly anisotropic phases (Dong, Kimura et al. 1996). This effect is attributed to electrical double-layer, as a decrease in double layer thickness leads to an increases the chiral interactions between the crystallites. (Dong and Gray 1997). In addition to inorganic cations, amines and ammonium ions have been coordinated to the surface sulfate groups to tune the aggregation behavior of CNC, mainly tuning the critical concentration for anisotropic phase formation. (Dong and Gray 1997) In later years, Vignolini et al. (2014, 2022) established a quantitative link between colloidal liquid crystalline behavior and the morphological distribution of individual CNC particles, and found that CNC-crystallite aggregates, or ‘bundles,’ act as colloidal chiral dopants, directly affecting the chiral nematic pitch. By using ultrasonication to reduce bundle size, they increased the pitch and induced a red shift toward longer wavelengths in dried films. (Dumanli, van der Kooij et al. 2014, Parton, Parker et al. 2022) These findings were applied and further explored in *Paper II* and alongside other projects. The use of Az-salts for the modification of sulfonated CNC was studied in *Paper III*, in relation to the alkyl chains influence on CNC arrangement in suspensions and films.

3.4 Mueller Matrix Polarimetry (MMP)

The Mueller matrix represents all the consequences of the interaction of the incident polarized light with an anisotropic medium by treating Stokes vectors, representing the polarization of light. In this project, the interaction of light with CNC is studied to assess how CNC organizes in film with and without additives upon drying. Specifically, circular and linear dichroism are used to determine how CNC particles are organized into nematic-, smectic, chiral nematic, and other organized phases. The circular dichroism (CD) signal is used to differentiate between the different chiral regions in a molecule. If more left-handed light is absorbed compared to right-handed light, the CD signal is said to be positive. In this setup, a positive signal results from greater absorption of left-handed circularly polarized light, whereas a negative signal results from greater absorption of right-handed circularly polarized light.

The linear dichroism (LD) provides information about alignment in relation to the transition dipole moment within the molecule/particle, relative to an orientation axis. A positive signal indicates that the transition dipole moment is aligned parallel to the polarized light's direction. A negative signal indicates that the transition dipole moment is aligned perpendicular to the polarized light’s direction. Yet, some caution shall be taken in characterization from CD spectroscopy, as the CD signals often overlap with signals from linear dichroism (LD) and linear birefringence (LB).

CHAPTER 4
MATERIALS AND EXPERIMENTAL TECHNIQUES

This chapter describes the materials and methods used for the different papers. Some techniques are specific to fibers (Manuscript I) or CNC (Papers II and III). The experimental methods are hence divided into common techniques, fiber-specific techniques, and CNC-specific techniques.

4.1 Materials

Never dried softwood bleached kraft pulp (BKP_{ND}) was kindly provided by Billerud Korsnäs (Sweden) and used as delivered or liquid exchanged with ethanol and acetonitrile before use (BKP_{LE}). A carbohydrate analysis of BKP_{ND} revealed a relative glucose content of 80%, hemicellulose of 18.4%, and lignin content of 1.6%. BKP_{LE} was found to be 86% glucose, 12.3% hemicellulose, and 1.7% lignin. Avicel, MCC from cotton linter, was purchased from Sigma Aldrich and used without further modifications.

CNC-SO_3H was synthesized by hydrolysis of microcrystalline cellulose, MCC (Avicel PH-101) using 64 wt.% sulfuric acid. The dry weight was determined for each dilution and titrated to determine the sulfate half-ester content.

4.2 Chemical modifications

For the modification of BKP with itaconic anhydride, several methodologies and reaction conditions were explored. In all cases, the pulp is heated to facilitate reaction, although some room-temperature reactions were performed. In literature, mechanochemical reactions have gained interest, but are generally conducted using some sort of coupling agent or halide. Similarly, gas-phase reactions have been explored using acyl chlorides (David, Gontard et al. 2019), which might not be the best solution for industry applications, as HCl is formed during reaction. The gas-phase reaction of pulp was also explored by Malmgren and Nordqvist in 2023 for patent applications, using anhydrides instead of acyl chlorides, effectively esterifying cellulose pulp (Malmgren and Nordqvist 2023).

4.2.1 Manual Kneading, BKP_{ND} and BKP_{LE} Kn-reactions

Manual kneading reactions are mechanochemical reactions where, in this case, the reagent is kneaded into the pulp by hand before heating. Sjölund et al. (2025) compared mechanical kneading with hand kneading for the modification of pulp fibers and found that, although mechanical kneading resulted in a higher degree of substitution, it also led to a reduction in the crystallinity of the material (Sjölund, Westman et al. 2025).

In this project, both never-dried BKP (BKP_{ND}) and liquid exchanged-BKP (BKP_{LE}) were modified using itaconic anhydride. For reactions with $BKP_{ND,}$ the anhydride is directly put in contact with water, initiating the hydrolysis into H_2IA. After the incorporation of ITA with the pulp, the reaction is placed in the oven at the desired temperature and time. Upon heating, the acid reforms the anhydride, which then may react with the hydroxyl group of the fiber or be re-hydrolyzed back into the acid. Therefore, an equilibrium exists between the reformation of anhydride and consequential hydrolysis or reaction with the hydroxyl groups of the fibers. When BKP_{LE} is used, theoretically no or little water should be present in the structure, mitigating the hydrolysis of the anhydride into acid, thereby yielding a higher degree of substitution. Table 1 summarizes the different reaction conditions investigated for the esterification of BKP with ITA. The esterification reactions facilitated through kneading were also performed on MCC as a comparison. Molar ratios and water content were kept the same as in the experiments performed on $BKP_{ND/LE}$.

Table 1. Reaction conditions for kneading reactions, BKP_{ND} and BKP_{LE}, with ITA of different molar ratios (AGU:ITA), temperature, and drying time.

Sample label	**Fiber mass dry (g)**	**Molar ratio (AGU: ITA)**	**Temp. (°C)**	**Time**
BKP_{ND}				
BKP_{ND} Kn_1_RT_1g	1	1	RT	24 h
BKP_{ND} Kn_1_50 °C_1g	1	1	50	24 h
BKP_{ND} Kn_0.5_50 °C_1g	1	0.5	50	24 h
BKP_{ND} Kn_1_80 °C_1g	1	1	80	24 h
BKP_{ND} Kn_0.5_80 °C_1g	1	0.5	80	24 h
BKP_{ND} Kn_0.5_50 °C_12g	12	0.5	80	24 h
BKP_{ND} Kn_1_105 °C_1g	1	1	105	24 h
BKP_{ND} Kn_0.5_105 °C_1g	1	0.5	105	24 h
BKP_{LE}				
BKP_{LE} Kn_0.2_70 °C_1g 0 min, RT only	1	0.2	RT/70	0 min
BKP_{LE} Kn_0.2_70 °C_1g_10 min	1	0.2	70	10 min
BKP_{LE} Kn_0.2_70 °C_1g_20 min	1	0.2	70	20 min
BKP_{LE} Kn_0.2_70 °C_1g_30 min	1	0.2	70	30 min
BKP_{LE} Kn_0.2_70 °C_1g_60 min	1	0.2	70	60 min
BKP_{LE} Kn_0.2_70 °C_1g_120 min	1	0.2	70	120 min
BKP_{LE} Kn_1_70 °C_0.5g	0.5	1	70	30 min
BKP_{LE} Kn_0.2_70 °C_0.5g	0.5	0.2	70	30 min
BKP_{LE} Kn_0.1_70 °C_0.5g	0.5	0.1	70	30 min
BKP_{LE} Kn_0.05_70 °C_0.5g	0.5	0.05	70	30 min
BKP_{LE} Kn_0.035_70 °C_0.5g	0.5	0.035	70	30 min
BKP_{LE} Kn_0.025_70 °C_0.5g	0.5	0.035	70	30 min
BKP_{LE} Kn_0.020_70 °C_0.5g	0.5	0.020	70	30 min
BKP_{LE} Kn_0.2_70 °C_12 g	12	0.2	70	2h
BKP_{LE} Kn_0.1_70 °C_60 g	60	0.1	70	8h

4.2.2 Gas Phase Reactions

Gas phase reactions are conducted as the name states, in the gas phase. In general, gas-phase reactions refers to one or both reagents being transformed to the gas phase using pressure or heating. In this study, pulp is kept as a solid whilst itaconic anhydride is vaporized. The melting point of ITA lies around 74 °C, but a shift from solid to gas occurs earlier. The reactions in this project are conducted at 50 – 70 °C at constant volume, varying the partial pressure of the anhydride slightly by varying the temperature.

Heating to just 50 °C seems sufficient for the gasification, enabling the reaction with pulp in a solvent-free manner. Figure 15 illustrates the reaction setup. Inside the desiccator, a petri dish containing ITA is placed at the bottom. A metal sieve is positioned above the dish without touching the anhydride. Fluffed BKP_{LE} (prepared by blending for 3 × 10 seconds with a kitchen blender) is then placed on top of the sieve. The desiccator is sealed and placed in a preheated oven at the desired temperature for 22 hours. During heating, the ITA vaporizes and comes into contact with the hydroxyl groups in the fibers.

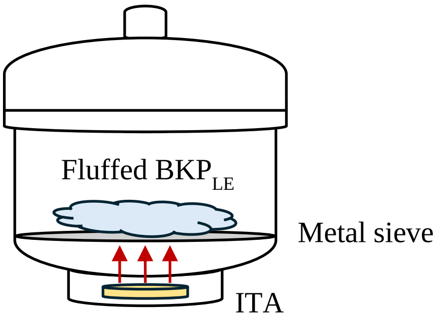

Figure 15. Illustration of gas-phase reaction. ITA is placed in a petri dish at the bottom of the desiccator. A metal sieve is in the desiccator, suspending the fluffed BKP_{LE} fibers over the anhydride without direct contact between ITA and fiber.

Table 2 summarizes the reactions performed for gas-phase reactions. The partial pressure of ITA is calculated using the ideal gas law (Equation 1) and is merely seen as an approximation for comparison.

$$PV = nRT \tag{1}$$

Where P is the pressure (Pa), V is the volume of the dessicator (2.8 dm^3), n is moles, R is the ideal gas constant ($m^3PaK^{-1}mol^{-1}$), and T is temperature (K). The partial pressure of ITA (P_{ITA}) can then be calculated due to the mole fraction (n_{ITA}) and total pressure of the system (P_{tot}) at the set temperature according to Equation 2.

$$P_{ITA} = n_{ITA} * P_{tot} \tag{2}$$

The partial pressure of ITA should in theory influence the degree of modification, as ITA can penetrate the fiber surface better at higher pressure.

Table 2. Reaction conditions for gas-phase reaction. All reactions were performed using the same desiccator for 22h. The partial pressure was calculated using the ideal gas law as is seen as an approximation.

Sample label	**Mass cellulose (dry, g)**	**Molar ratio anhydride (AGU: ITA)**	**Partial pressure anhydride (kPa)**	**Temperature (°C)**
BKP_{LE} Gas_1_75 °C_2g	2	1	11,5	75
BKP_{LE} Gas_0.1_75 °C_2g	2	0.1	1,3	75
BKP_{LE} Gas_0.01_75 °C_2g	2	0.01	0,13	75
BKP_{LE} Gas_1_50 °C_2g	2	1	11,0	50
BKP_{LE} Gas_1_75 °C_10g	10	1	11,0	75
BKP_{LE} Gas_0.2_150 °C_12g	12	0.2	-	150

4.2.3 Modification and alignment of CNC

For *Paper II*, different counter ions were used to coordinate to the sulfate groups on CNCs. As previously stated, counterions are known to influence colloidal and thermal stability, as well as flexibility, due to their influence on aggregation, packing, and alignment. In *Paper II*, H^+, Na^+, and Et_4H^+ were used as they all are monovalent but have different sizes and spatial occupancy. Na^+ was introduced through the addition of NaOH (1:1 molar ratio of sulfate half ester to Na^+), Et_4N^+ as pure amine, and H^+ from HCl, adjusted to a pH value around 3.

The findings from *Paper II* triggered an application to the beamline B23 at Diamon Light Source, UK, to further understand the correlation between additives and organization of the CNCs. In the studies conducted at the beamline, from here denoted as B23-MMP, pristine CNC-OSO_3H, CNC-OSO_3H_Triethanolamine (TEOA), CNC-OSO_3H_TEOA_Glycerol (Gly), and CNC-OSO_3H_TEOA_N-Methylimidazole (NMIM) films were researched in relation to their optical properties using MMP analysis. The additives of choice were used to create intermolecular interactions, thereby ordering the CNCs in different manners. A summary is presented in Table 3. Glycerol is commonly used in polysaccharides as a plasticizer (Fernández-Santos, Valls et al. 2021), coordinating to the hydroxyl groups, and NMIM is known to coordinate to axial C-H’s on carbohydrates (Kiessling and Diehl 2021).

Azetidinium salts (Az-salts) were used to react covalently with the sulfate half ester on CNCs, altering their properties by introducing alkyl chains to their surface, as discussed in *Paper III*. Az-salts were synthesized through the reaction of epichlorohydrin (ECH) and a secondary amine, illustrated in Figure 16. The 3-chloro-2-hydroxypropyl structure is synthesized at ambient temperature for 12 h in iPrOH. The ring-closing step is performed in iPrOH/H_2O mixture (1:10), at 80 °C.

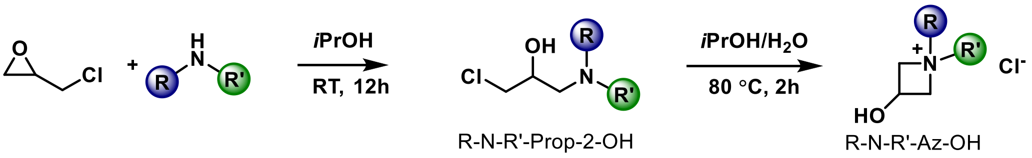

Figure 16. Synthesis of Az-salts from ECH and dialkylamine, forming firstly the 3-chloro-2-hydroxypropyl structure before closing to the Az-salt.

The conjugation of Az-salt to CNC-SO_3H is made through the addition of Az-salt to the CNC suspension, and heating for 2h at 80 °C. The Az-salts synthesized and used for the modification of CNC are presented in Figure 17.

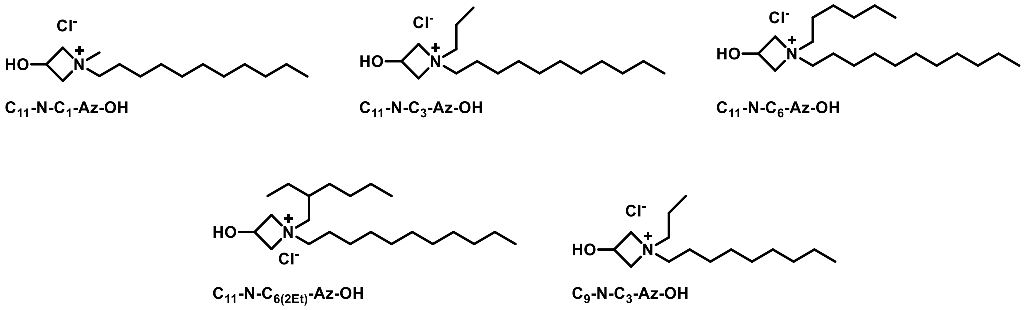

Figure 17. Synthesized and used Az-salts for the conjugation with CNC.

Table 3 summarizes the different CNC reactions in the different papers based on CNC origin, that is in in-house produced or purchased Celluforce, sulfate content, and weight percent in film or gel. It shall be noted that in-house CNC was prepared from MCC, source cotton, whereas Celluforce-CNC is produced from softwood kraft pulp. Noteworthy is that the Celluforce crystals are larger than those of the in-house CNC. Additionally, the chemical additives are listed and the molar ratio of sulfate to additive is given. For *Paper II*, different drying conditions of the films were investigated, divided as:

i. Left to dry for several days in a fume hood at ambient conditions
ii. Left for ~24 h in a 45 °C oven, denoted 45 and Son-45 for suspensions that were sonicated.
iii. Left for a week in an evacuated desiccator, denoted Vac and Son-Vac for suspensions that were sonicated.

Different concentrations (wt.%) of CNC suspensions were used in the different studies. Generally, when wanting to study the chiral nematic arrangement of CNCs, a higher concentration is used due to them being nearer the gel point. Lower concentrations of CNC suspensions were used in the B23-MMP project, as reduced concentrations exhibit less aggregation and CNC-CNC interaction, thereby facilitating a clearer assessment of the effects of additives.

Table 3. Summary of CNC experiments conducted for respective studies. The charge was determined through titration or provided by the manufacturer. The weight fraction is given for films and/or suspensions depending on the paper.

CNC origin	**CNC-OSO$_3^-$ H$^+$ Charge (μmol/g)**	**wt.% suspension (g/g)**	**Additive/Counterion**	**Molar ratio (sulfate:additive)**
Paper II				
CelluForce,	280 μmol/g (0.0465/AGU)	2.5	H$^+$	1
			Na$^+$	1
			Et$_4$N$^+$	1
In house	300 μmol/g	2.69	H$^+$	1
			Na$^+$	1
			Et$_4$N$^+$	1
Paper III				
In house	330 μmol/g	1.0	-	-
		1.5	-	-
		2.0	-	-
		3.0	-	-
		4.0	-	-
		5.0	-	-
		1.5 and 3.0	C$_{11}$-N-C$_1$-Az-OH	1
		1.5 and 3.0	C$_{11}$-N-C$_3$-Az-OH	1
		1.5 and 3.0	C$_{11}$-N-C$_6$-Az-OH	1
		1.5 and 3.0	C$_9$-N-C$_3$-Az-OH	1
		1.5 and 3.0	C$_{11}$-N-C$_{6(2Et)}$-Az-OH	1
B23-MMP series, manuscript in preparation				
In house	316 μmol/g	1.1	-	-
			TEOA	1.1
			TEOA Gly	1.1
			TEOA NMIM	1.1

4.3 General Characterization Techniques

The following techniques were used both in CNC and fiber projects and are hence presented together. Two other subsections explain the methods used specifically in fiber or CNC work respectively. Some techniques, such as TGA or CP/MAS ^{13}C NMR may be employed for both fibers and CNC but are only used for one of the systems and is hence presented in the respective section.

4.3.1 FTIR

The ATR-FTIR spectra were collected on a Vertex70v FTIR spectrometer, 4000-400 cm^{-1}, 32 scans with a resolution of 4 cm^{-1}. The background was collected before the recording of spectra and subtracted from the collected data. Baseline correctionns were performed using the software, and the data was normalized to the cellulose glycosidic bond (C–O–C) antisymmetric stretching vibration at 1160 cm^{-1} (Salmén and Stevanic 2018). The first derivative plots were calculated and produced using Origin, using normalized data. The carbonyl and alkene regions were evaluated to assess reaction outcomes.

4.3.2 Potentiometric and conductometric titration

For the charge assessment of CNC in *Paper II* and *III* conductimetric titration was used. Each sample was sonicated before use and NaCl was added to ensure conductivity. The surface charge was calculated based on the equivalence point of the curve. 0.1M NaOH was used as a titrant, using a Titrando 905 Methrom setup. Specifically, 0.4 wt.% samples were used and sonicated for 30-60 seconds before titration and 40 µmol NaCl (0.5M) was added. The sulfate content was calculated as in Equation 3.

$$Sulfate\ content\ \left[\frac{mmol}{g}\right] = \frac{c_{NaOH} * V_{NaOH}}{m_{CNC}} \tag{3}$$

Where c_{NaOH} is the concentration of NaOH (M), V_{NaOH} is the volume consumed at the equivalence point (mL), and m_{CNC} is the dry mass of CNC in the sample (g). The same assessment of charge was made for CNC suspensions used in the B23-MMP project, but using potentiometric titration instead.

For the assessment of fiber charge, here, carboxylic acid from the itaconic-group, potentiometric titration was used due to its sensitivity towards different carboxylic acid groups on the fiber surface. Approximately 20 mg of dry fibers were spun in MQ-water overnight before titration to resuspend and swell the fibers. 40 µl NaCl (0.5M) was added alongside a known amount of 1M HCl to lower the pH to between 2.7-3.2 for full protonation of the sample. The charge was calculated based on the last determined equivalence point for the titration and corrected for the addition of HCl according to Equation 4.

$$Carboxylic\ acid\ \left[\frac{mmol}{g}\right] = \frac{c_{NaOH}(V2 - V1)}{m_{fibers}} \tag{4}$$

Where V1 is the volume of NaOH (mL) needed to neutralize the known amount of HCl added, V2 is the volume of NaOH (mL) at the last equivalence point, c_{NaOH} is the concentration of NaOH (M), and m_{fibers} (g) is the dry mass of fibers titrated. (Beatson 1992, Lindgren, Öhman et al. 2002, Åhl, Ruiz-Caldas et al. 2025). In the following fiber-related section, the carboxylic charge is expressed as milli-equivalence per gram of fiber and is taken as 1:1 due to the 1:1 relationship between carboxylic acid group and NaOH. That is, mmol/g = meq/g. The degree of substitution is calculated as the ratio of itaconic groups per hydroxyl group on the AGU, according to Equation 5.

$$DS\ \left(\frac{substitution}{OH\ on\ AGU}\right) = \frac{n_{sub}}{3 * \left(\frac{1}{M_{AGU}}\right)} \tag{5}$$

Where n_{sub} is the carboxylic acid content (mol/g fiber), M_{AGU} is taken as 162 g/mol, multiplied by 3 as each AGU contains 3 hydroxyl groups.

4.3.3 Dry weight

The dry weight of fibers and CNC is determined prior to modifications as fibers are delivered wet, and CNC are kept in water suspension of different concentrations for different applications. The dry weight is determined by the ratio between dry (m_{dry}) and wet (m_{wet}) matter. Samples are weighed onto dry petri dished before drying in oven (105 °C for fibers, 60-80 °C for CNC). The dry weight is given as in Equation 6.

$$wt\% = \frac{m_{dry}}{m_{wet}} * 100 \tag{6}$$

4.3.4 SEM

SEM images of fibers and CNC in *Paper II* were taken using the SEM - Zeiss Ultra 55 FEG. Samples were stuck on carbon tape before coating through sputtering, with 4 nm of gold. The secondary signal was collected for imaging, with an acceleration voltage between 10-15 kV.

SEM images of the cross-section of CNC films for the B23-MMP project were taken on a SEM - JEOL JSM-7800F Prime, at 1kV. Samples were glued to silica plates using silver paint, split, and glued perpendicular to the SEM stub to investigate the cross-section of the CNC film.

4.3.5 NMR

Solution NMR was performed on a 400 MHz spectrometer in chloroform-d and DMSO-d_6 for the 3-chloro-2-hydroxypropyl and Az-salts, respectively. Analysis was performed using MestreNova.

4.3.6 X-Ray Diffraction, PXRD

All measurements were performed on a Bruker D8 Advance instrument with Cu-Kα radiation of 1.54 Å. All samples were mounted on a zero-background silica single crystal holder for data collection. For CNCs in *Paper II*, data in the range of $10° \leq 2\theta \leq 50°$ was collected. The Crystallinity Index (CI) of cellulose samples was measured by Equation 7, comparing the crystalline signal to the total area (Daicho, Saito et al. 2018).

$$Crystallinity\ index\ (CI) = \frac{Area_{Crystalline}}{Area_{Total}} * 100 \tag{7}$$

For fibers, data was collected between $5° \leq 2\theta \leq 55°$. To evaluate the average crystallite size (L) for each sample, the signal from the (200) reflection plane was fitted with a Gaussian function, and the Scherrer equation was used, as in Equation 8.

$$L = \frac{0.9\lambda}{\beta cos\theta} \tag{8}$$

Where λ is the incident X-ray wavelength, β is the full width at half maximum (FWHM) of the Gaussian curve fitted to the (200) reflection in radians, and θ is the position of the signal maximum of the (200) reflection, also in radians. 0.9 is taken as a shape factor specific to cellulose. (Scherrer 1918, Patterson 1939, French and Santiago Cintrón 2013, Agarwal, Ralph et al. 2017)

4.3.7 Tensile testing

For CNC films, an Instron Tensile Tester was used with a strain rate of 2mm/min. CNC films of 4cm x 1cm were prepared according to ASTM D882-12 standards and measured with a 2cm gage length. The thickness of the films was measured in triplicate using a Mitutoyo micrometer, with six replicate films analyzed for each film type.

For fibers, a Zwick tensile tester was used according to ISO-15754. Sheets of the fibers were made and left to acclimate at 50% RH and 23 °C for 48h before being cut into strips (15 mm wide) for testing. The thickness of the acclimated sheets was measured in triplicate for each sheet used to make strips. In total, 3 sheets of each type were used for tensile testing.

The tensile index, σ_T^W, is commonly used in paper and fiber testing to measure the strength of paper relative to its basis weight (mass per unit area), as shown in Equation 9, Where F_T is the tensile strength, *b* is the width of the paper strip, and *w* is the grammage of the paper (g/m^2)

$$\sigma_T^W = \frac{F_T}{b * w} \tag{9}$$

4.4 Fiber-Specific Characterization Techniques

This section presents methods used in *Manuscript I*. Some of these methods may generally also be used to study CNC but were not used in *Papers II, III*, or other CNC work (B23-MMP).

4.4.1 Klason Carbohydrate Analysis

Carbohydrate analysis was performed to determine the content of cellulose, hemicelluloses, and lignin in the used pulp, BKP. The method by Kron et al. (Kron, Marion de Godoy et al. 2023) was used for the analysis. In general, samples were hydrolyzed to disintegrate all polysaccharides and separate them from the remaining lignin. The samples were analyzed using an anion exchange chromatography with pulsed amperometric detection.

4.4.2 Polyelectrolyte titration

Polyelectrolyte titration is a method used to assess charge distribution on fibers by adsorbing polymer onto or into the fiber. This method enables the localization of the charges and is based on the work of Winter et.al (Winter, Wågberg et al. 1986). Different sizes of polymers will be able to adsorb to different parts of the fibers, as they may be too large to penetrate the fiber wall, not reaching the charges localized there. Poly (diallyldimethylammonium) chloride (polyDADMAC) is used for the determination of surface charges, whilst poly(hexadimethrine) bromide (polyBRENE) is used for the total charge assessment. The fibers are allowed to absorb a pre-decided polymer loading for the desired time before filtration. The filtrate is titrated to gain the remaining polymer amount not adsorbed. The procedure is repeated a minimum of 5 times with different polymer concentrations, creating a sorption isotherm which can be used to calculate the amount of absorbed polymer at equilibrium.

4.4.3 Water Retention Value, WRV

To estimate the water binding capacity of the samples, water retention values were measured by a method of Börjesson et. al., adapted for this study. (Borjesson, Richardson et al. 2015) Approximately 100 mg of pulp was suspended in deionized water for 4h, after which the fibers were placed on a filter (pore size of 45µm) within a centrifuge tube and allowed to drip freely overnight. Thereafter, the self-dripped water was discarded, and the fibers were spun through centrifugation for 15 minutes at 3000 G. The fibers were weighed, gaining $m_{\text{wet fibers}}$ before placement in an oven for drying at 105 °C for 24h, $m_{\text{dry fibers}}$. The WRV was calculated based on the wet and dry mass of the pulp as Equation 10.

$$WRV = \frac{m_{wet\ fibres} - m_{dried\ fibres}}{m_{dried\ fibres}} \equiv \frac{m_{water}}{m_{dried\ fibres}} \tag{10}$$

A higher value corresponds to higher absorbing properties, such as g water/g cellulose. Triplicates were performed for each sample.

4.4.4 Tea-Bag Value, TBV

The tea-bag tests were performed in triplicate for each sample. For this, 100 mg fibers were swelled in 20 mL of water for 4h, before allowing them to drip through the centrifuge filter (pore size of 45µm). Once dripping had ceased, the fibers were weighed (m_{wet} fibers after dripping), spun, and dried at 105 °C ($m_{\text{dried fibers}}$) to assess their water-holding capacity. The tea-bag value was calculated as in Equation 11.

$$Tea - bag\ value = \frac{m_{wet\ fibres\ after\ dripping}}{m_{dried\ fibres}} \tag{11}$$

4.4.5 CP/MAS ^{13}C NMR

CP/MAS ^{13}C-NMR spectra were recorded on pulp fibers which were packed at ambient conditions in zirconium rotors. The samples were ran at 298 K on a Bruker Avance III 500 MHz spectrometer, equipped with a 4mm HX CP/MAS probe. A contact time of 1.5 ms and repetition time of 2 s was used at a magic angle spinning rate of 10 kHz. 4000 scans were collected for each sample. The dataset was normalized to have the same intensity at the 89 ppm signal to explore the C4 region of the spectra. Spectra were analyzed using TopSpin 3.7.0.

4.4.6 Sheet formation

Sheets were formed from the modified and unmodified BKP to investigate tensile strength and processability. A semi-automatic Rapid Köthen Sheet former was used to produce sheets with a grammage of 60g/m^2. The pulp was disintegrated at 30,000 revolutions before use.

4.5 CNC Specific Characterization Techniques

This section summarizes methods used in Papers II and III, and other techniques used for the studies of CNC.

4.5.1 Preparation of films by solution casting method

CNC films were prepared in both *Paper II* and the B23-MMP project. In general, approximately 20 ml of 1 wt.% CNC is used for one film and dried in petri dishes at ambient temperatures, but different conditions apply for different projects. Samples were, in general, sonicated right before casting to generate even films and allow self-aggregation. In *Paper II*, the effect of sonication was studied, and samples were sonicated either cooled or at ambient temperatures.

4.5.2 Zeta Potential

In *Paper II*, the hydrodynamic diameter of CNC was measured on a Zetasizer Nano ZS (Malvern Instruments, Malvern, UK) using dynamic light scattering (DLS) with a 50 mW diode-pumped solid-state laser as a light source. The scattering angle was set to 173°. The Smoluchowski approximation for larger particles with a relatively thin double layer was used to estimate zeta potential from electrophoretic mobility. Samples were prepared with the same ratios as the films, but with 0.25 wt.% CNC. *Paper III* also utilized DLS measurements, using CNC with a concentration of 0.01 wt.% at 25 °C.

4.5.3 Wettability and swelling

In *Paper II*, the wettability of CNC was measured using contact angle measurements and bulk swelling. For the contact angle, an optical goniometer from Attention was used. The bulk swelling was measured by immersing three pieces of the CNC sample (each sample of 2 cm × 2 cm) in DI water in a Petri dish for 1 h. The absorbed water or swelling percentage was calculated using Equation 12.

$$S(\%) = \frac{W_s - W_d}{W_d} * 100 \tag{12}$$

Where W_s is the swollen weight and W_d is the weight after drying.

4.5.4 TGA

TGA analysis was performed for different CNC films in *Paper II* and *III*. Samples were measured from 30 to 500 °C, with a heating rate of 10 °C/min.

4.5.5 Polarized Optical Microscopy

Polarized optical microscopy (POM) was used to study CNC films in *Paper II*. Images were taken on a Zeiss Axio Scope.A1 (Oberkochen, Germany) with linear polarizers in a cross-polarizer setup in brightfield mode and magnification lenses 20x, 40x, and 100x.

4.5.6 UV-Vis light spectroscopy

UV-Vis was used to study CNC films in *Paper II*. A PerkinElmer Lambda 950 UV-vis spectrophotometer was used, with air as a background from 300 to 800 nm wavelength. The central part of each film was placed in the upper part of the window in the sample holder at a 90° angle to the incident light. Replicates were taken of samples with visible variations in translucency, and a sample corresponding to an intermediate value was selected for reporting the result.

4.5.7 Rheological Characterization

Rheological measurements were performed for CNC-suspensions in *Paper III*, conducted in collaboration with Roland Kádár and his research group at Chalmers University of Technology, Gothenburg, Sweden. Linear and nonlinear oscillatory shear measurements were performed on the suspensions. All experiments were conducted at 23 °C, and each sample was allowed to relax for 300 s after moving to the gap position (1 mm). Strain sweep measurements were performed within a strain amplitude range of 0.01% to 1500% at the following angular frequencies: 0.6, 1, 2, and 4 rad/s. Frequency sweep tests were performed between 600 and 0.01 rad/s at an imposed strain amplitude of 0.3%. The strain amplitude was selected based on the strain sweep tests so that it was in the linear viscoelastic region.

4.5.8 MMP - Mueller Matrix Mapping and Measurement

Mueller Matrix Polarimetry (MMP) measurements were conducted at the B23 beamline at Diamond Light Source, UK, and is a method used to study polarization properties of materials. In this project, CNC films containing different additives to CNC-OSO_3^- were studied to understand the alignment and aggregation of. To gain the Mueller Matrix for the respective samples, one wavelength is used to raster scan the whole sample. For this, a random point was chosen to measure the absorbance of light and determine a suitable wavelength for the scanning of the whole film, to have adequate absorbance and detectable signals. Each film was measured as 2x2 mm area with 41x41, 50 micrometer resolution, generating data for the MMP maps. The produced maps are transformed into a 3x3 matrix containing the CD, LD, LD’ CB, LB, LB’, Abs E-factor, and DI. Depending on the decoupling constant, DI, different approaches of the MMP were used as the data can be interpreted analytically, by the matrix method, or independently.

CHAPTER 5
RESULTS – FIBER MODIFICATION

This chapter summarizes the findings from Manuscript I, the influence of the esterification of cellulose fibers on their chemical and material properties.

5.1 Esterification of cellulose fibers

The chemical modification of BKP through different reaction conditions was assessed using ATR-FTIR, potentiometric and polyelectrolyte titration, WRV, TBV, CP/MAS ^{13}C NMR and PXRD. Prior to modification with ITA, carbohydrate analysis was performed on BKP_{ND} and BKP_{LE} to gain a distribution of glucose, hemicelluloses and lignin. BKP_{ND} revealed a relative glucose content of 80%, hemicellulose of 18.4%, and lignin content of 1.6%, BKP_{LE} was found to contain 86% glucose, 12.3% hemicellulose and 1.7% lignin. Thus, the action of liquid exchanging the pulp with ethanol and acetonitrile seems to remove some of the hemicellulose.

5.2 FTIR

ATR-FTIR was used for the assessment of all reactions performed based on the strength of the carbonyl signal. For all modifications, two carbonyl signals, one ester and one carboxylic acid signal should appear alongside an alkene/vinylidende, originating from the conjugated itaconic acid. Carboxylic esters usually express signals in the 1750-1735 cm^{-1} region whilst α, β-unsaturated esters present bands around 1730-1715 cm^{-1} and carboxylic acids around 1710-1760 cm^{-1}. Other adjacent groups and their electronic state may further influence the signal frequency. The vibrations for out of chain alkenes/ vinylidenes occur between 1658-1648 cm^{-1}, whilst cis and trans disubstituted alkenes (as found in citraconic and mesaconic acid, respectively) are found between 1662-1625 cm^{-1} and 1678-1668 cm^{-1}. (Pavia, Lapman et al. 2015) The types of counter ion are also important for the assessment of FTIR spectra. Carboxylates, deprotonated carboxylic acids, present around 1600 cm^{-1} and 1400 cm^{-1} (Pavia, Lapman et al. 2015), much lower than the protonated acids. The counter ion or state of protonation also seems to consequently influence the vibrational frequency of the adjacent alkene.

As discussed by Cortes Ruiz et al. (2025) in the esterification of fully bleached Norwegian spruce fibers with maleic anhydride, a shift for the alkene in the structure occurred, moving from 1638 cm^{-1} to 1616 cm^{-1} from protonated to deprotonated form of the carboxylic acid, respectively. The protonation state of the carboxylic acid did not affect the frequency of the ester which remained at 1719 cm^{-1}. The C=O frequency for the carboxylic acid seemed to be shifted from overlapping with other carbonyls to 1578 cm^{-1} upon ionization (Cortes Ruiz, Martin et al. 2025). Zheng et al. also introduced maleic anhydride to cellulose fibers originating from northern softwood kraft pulp, finding characteristic signal at 1718 and 1577 cm^{-1}, here assigned to the C=O and $–COO^{-}$ groups respectively, not mentioning the alkene group. (Zheng, Zhu et al. 2025). A comparison is provided in Figure 18.

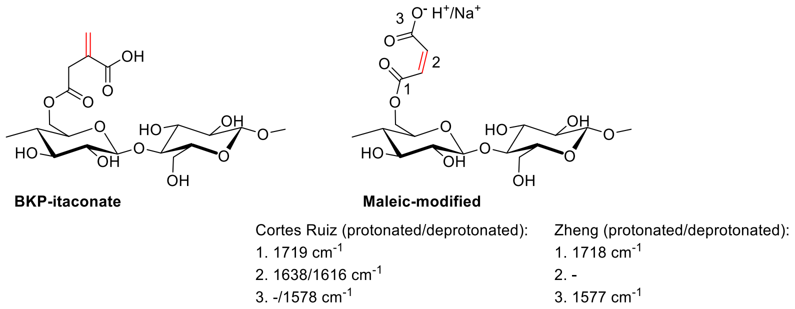

Cortes Ruiz (protonated/deprotonated):
1. 1719 cm^{-1}
2. 1638/1616 cm^{-1}
3. -/1578 cm^{-1}

Zheng (protonated/deprotonated):
1. 1718 cm^{-1}
2. -
3. 1577 cm^{-1}

Figure 18. Comparison of BKP-itaconate (left) and maelic anhydride modified cellulose. Note that more isomers are possible for BKP-itaconate, discussed in the following section.

Itaconic-modified BKP, from here on called BKP-itaconate, presents more and different signals compared to maleic modified cellulose. As previously explained, itaconic acid has the possibility to isomerize into both citraconic and mesaconic acid, although reported to occur at higher temperature. However, based on the FITR data collected in this project, it is indicated that the isomerization occurs also at lower temperature when conjugated to cellulose. A schematic is presented in Figure 19. Further, hydrogen bonding between cellulose fibers and itaconic acid may also shift the detected frequencies for the carboxylic acid and ester.

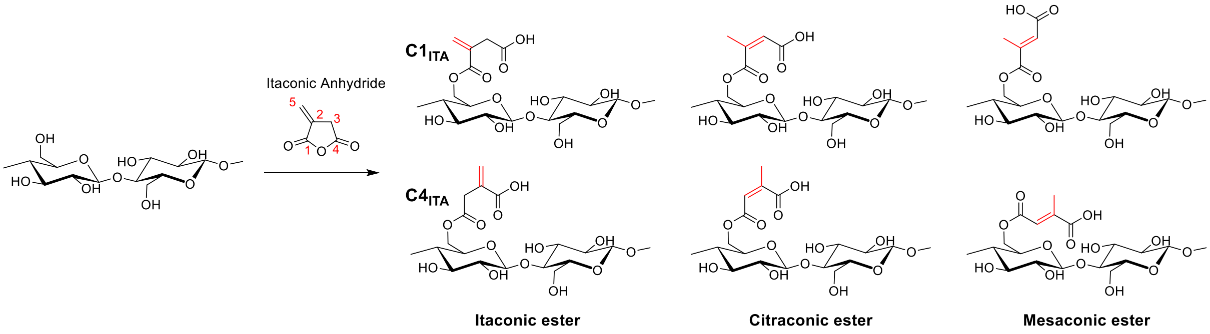

Figure 19. A schematic illustration of the different isomers thought to possibly appear on the BKP-itaconate.

The kneading reactions performed in *Manuscript I* were done on either BKP_{ND} or BKP_{LE} pulp. For BKP_{ND}, different drying temperatures were investigated. Ambient temperatures, 50 °C, 80 °C and 105 °C were explored with a drying time of 24h to fully dry the fibers. Molar ratios of 1:1 or 1:0.5 (AGU:ITA) were explored. Further, reaction sizes between 0.5g to 12g (dry) were used. In Figure 20 the FTIR spectra are presented for the different reactions.

The region between 1800 cm^{-1} and 1600 cm^{-1} is important because the carbonyl (C=O) stretch, which typically appears during esterification, is usually observed in this range. The success of the modification was determined by comparing the relative intensity of the carbonyl signal with the normalized 1160 cm^{-1} C-O-C signal of cellulose. The signal intensity is the highest for reactions performed at 105 °C, BKP_{ND} Kn_0.5_105 °C_1g, followed by BKP_{ND} Kn_1_105 °C_1g. Both samples showed significant hornification (fibers did not re-suspend after stirring in 50/50 acetone/H_2O for 48h) upon drying and were hence not used in forthcoming experiments and analysis. Reactions at 80 °C presented weaker carbonyl signals but no hornification, seen as fibers could be easily dispersed during the washing step. Reactions at 50 °C and ambient temperature showed weak to no carbonyl signals. This is most likely attributable to the temperature being too low to facilitate the re-formation of ITA. As previously discussed, ITA exists in equilibrium with H_2IA in the presence of water, and its regeneration is essential for the reaction to proceed. Consequently, no reaction is observed under these conditions. The frequency of the carbonyl for the BKP$_{ND}$ Kn-reactions seem to occur at 1710 cm^{-1} and 1725 cm^{-1}, with the signal at 1640 cm^{-1}, corresponding to water or the C=C bond from itaconic acid.

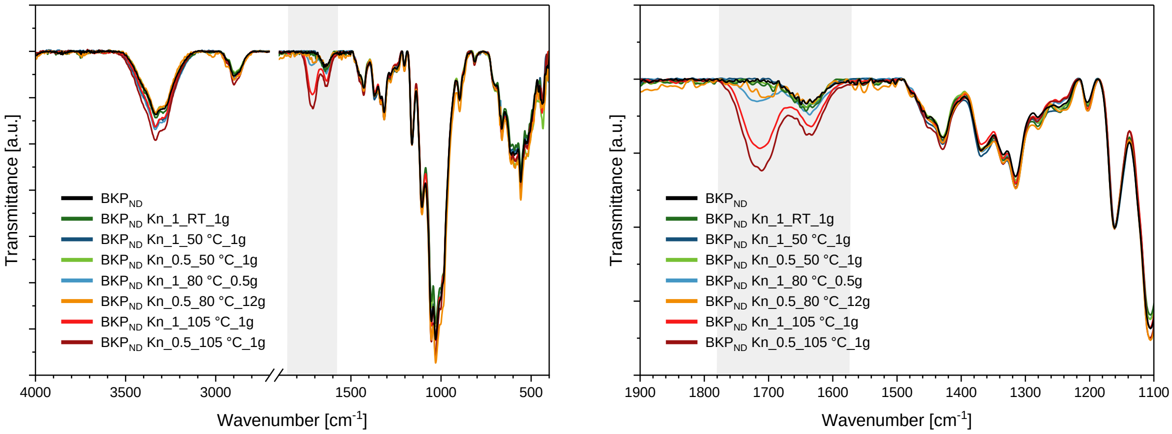

Figure 20. BKP$_{ND}$ Kn-reactions for different batches at different temperatures with varying molar ratios.

For BKP$_{LE}$ Kn-reactions, two optimizations were conducted based on the strength of the carbonyl signal. Firstly, the drying time at 70 °C was optimized for reaction sizes of 1g dry fibers and 1:0.2 molar ratio AGU:ITA. In Figure 21 the spectra for the reaction series are presented. From the graph, all reactions with different drying times present carbonyl signals. The drying time of 120 minutes, BKP$_{LE}$ Kn_0.2_70 °C_1g_120 min, gained the strongest signal, whilst drying times between 10 to 60 minutes gained similar results. The reaction performed without drying at 70 °C, only left on the bench until dry showed a weaker signal. Based on these findings, the standard drying time of 30 minutes at 70 °C was used for all smaller batches, 0.5-2g. For large batches, 10, 12 and 60g, the drying time was adapted as to evaporate all acetone, used to facilitate mixing of the ITA and BKP. In those cases, the sample was placed at 70 °C until no scent of acetone was left.

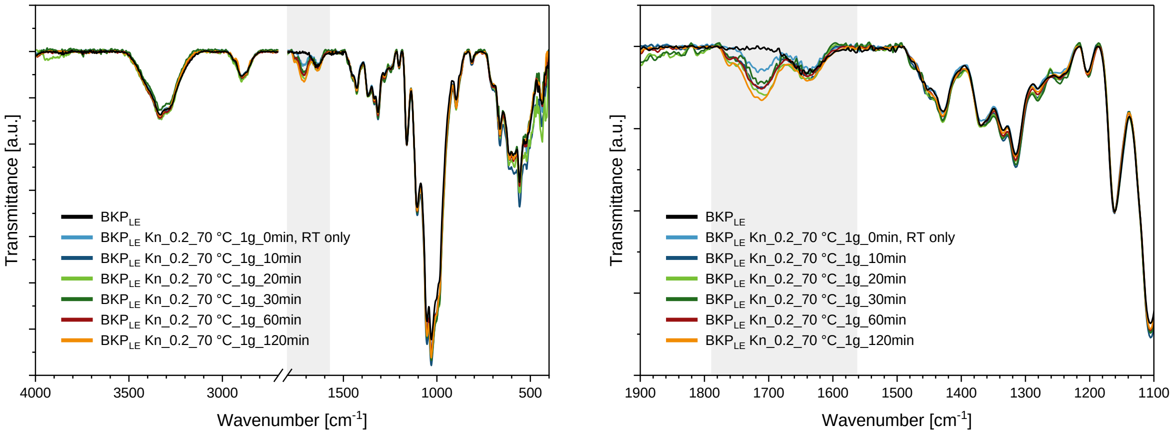

Figure 21. Reaction time optimization for BKPLE Kn_0.2_70 °C_1g_Xmin

The signals of the carbonyl group seem to shift slightly depending on the reaction conditions, with the highest intensity signal occurring at 1704 cm^{-1}/1717 cm^{-1} for (C=O) and a minor shoulder observed at 1762 cm^{-1}. The C=C bond again appears around 1632 cm^{-1}, with another signal at 1660 cm^{-1}, and again with a shoulder sometimes occurring around 1691 cm^{-1}. The variety in frequencies indicates both a ring opening at the C1 and C4 of ITA, as well as possible isomerization.

As presented in Figure 22, different molar ratio of AGU:ITA were explored, all conducted at 70 °C for 30 minutes. A 1:1 molar ratio gained the strongest carbonyl, closely followed by 1:0.2 molar ratio. Molar ratios below 1:0.05 were seen as unsuccessful. For large scale reactions a 1:0.2 molar ratio was used for economic and environmental reasons.

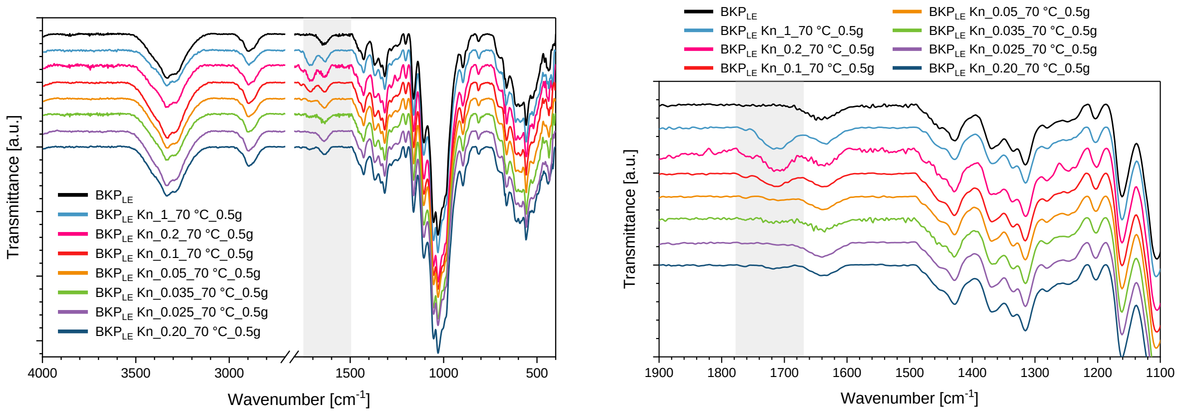

Figure 22. Optimization of molar ratios for BKPLE Kn_X_70 °C_30min

The gas-phase reactions were explored based on molar ratio and temperature. ITA melts at temperatures around 70-72 °C at normal pressure, and has a boiling point of 115 °C. In prior experiments conducted at elevated temperatures (150 °C), discoloration of the pulp was observed, which is undesirable as it compromises the material's suitability for further applications and chemical modifications. Accordingly, 75 °C was chosen as the operating temperature, as it allows ITA to melt and transition into the gas phase without causing discoloration of the fibers. A reaction time of 22 h was used to ensure the vessel reaching equal temperature all around. In Figure 23 the FTIR spectra of the different reactions are presented. A molar ratio of 1:1 at 75 °C, BKP_{LE} Gas_1_75 °C_2g showed the strongest signal intensities for the carbonyl group, followed by BKP_{LE} Gas_0.1_75 °C_2g. Further, 50 °C was tested with a 1:1 molar ratio, presenting a weaker carbonyl band of similar intensities as BKP_{LE} Gas_0.1_75 °C_2g. Molar ratio of 1:0.01 gained no carbonyl signal. As not all ITA is used in the gas-phase reaction, an approximative partial pressure of ITA in the desiccator was calculated, as explained in section 4.2.2. Based on those calculations, BKP_{LE} Gas_0.1_75 °C_2g and BKP_{LE} Gas_1_50 °C_2g should have the same partial pressure and hence similar degree of modification. This is consistent with the data from the FTIR spectra. For large scale reactions a molar ratio of 1:1 was used.

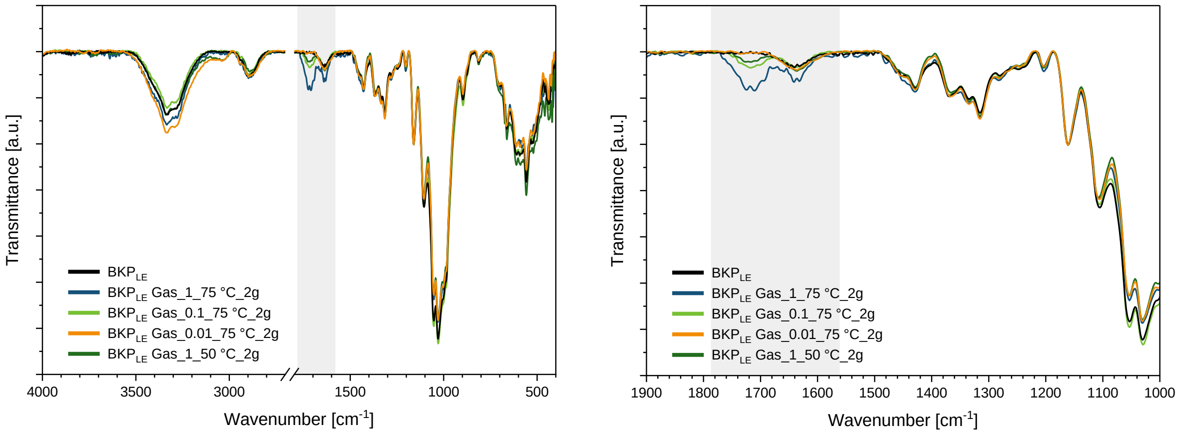

Figure 23. FTIR spectra for gas-phase reactions performed at different temperatures and molar ratios.

The relevant signals for the BKP_{LE} Gas-reactions are seen as the ester group exhibiting characteristic absorption bands around 1710–1725 cm^{-1}, with a minor shoulder observed near 1750 cm^{-1} in the BKP_{LE} Gas_1_75 °C_2g reaction spectrum. The C=C double bond appears around 1630 cm^{-1}, though this region slightly overlaps with the broad water absorption. Additionally, it is suspected that the carboxylic acid C=O stretch may also contribute to the signal in this region, as indicated by shoulders observed near 1693 cm^{-1}.

To gain deeper insight into the modification mechanism, particularly regarding changes in the C=O, C–H, and O–H regions, the first derivatives of the FTIR spectra were analyzed. In 1988, Michell established a correlation between the OH stretching frequencies in carbohydrate with hydrogen bonds or OH---O distanced in carbohydrates and found changes depending on the type of cellulose studied, I or II. He also examined the C–H absorption signals to gain additional insight into the structural characteristics of cellulose. (Michell 1988) Similarly, it should be possible to see differences between the different batches of BKP-itaconate compared to their respective references.

The C-H vibrations of the 2938 cm^{-1} signal were studied in the first derivative, but other regions near 2965, 2904, 2880 cm^{-1} are also of interest. The OH-active region between 3800 cm^{-1} and 3600 cm^{-1} was also investigated on trends correlating to the carbonyl band. In this project, the derivatives of the spectra were calculated on the baseline-corrected and normalized spectra.

Figure 24 presents the first derivative of the different reactions performed within the regions of interest, O-H and C-H, compared to the carbonyl region. In all reaction methods, clear changes are visible between the modified and the reference sample. Further, a strong change in signal in the carbonyl regions seems to correspond to a more convoluted O-H spectrum (3800-3600 cm^{-1}), indicating that the carbonyl groups play a crucial role in water holding capacities. The C-H region for the different samples and reaction conditions is slightly harder to decipher; however, looking at the 2938 cm^{-1} signal, changes are apparent for all samples compared to their references. In the case of BKP_{ND} Kn-reactions, a plateau is seen instead of a clear minimum, showing that change occurs in the C-H structure independently of the degree of modification, most likely due to an additional washing and drying cycle compared to BKP_{ND}. For the BKP_{LE} Kn-reactions, a small maximum found in the reference sample is changed to a plateau in all modified samples, again independently of the degree of modification or the molar ratio used during the modification.

BKP$_{ND}$ Kn - reactions

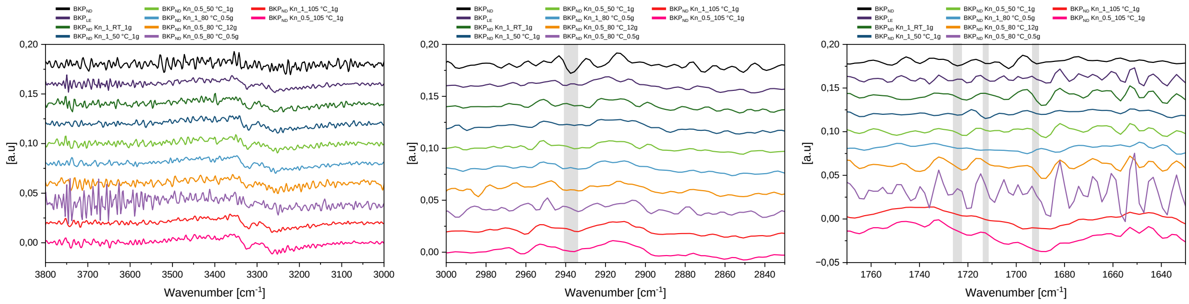

BKP$_{LE}$ Kn - reactions

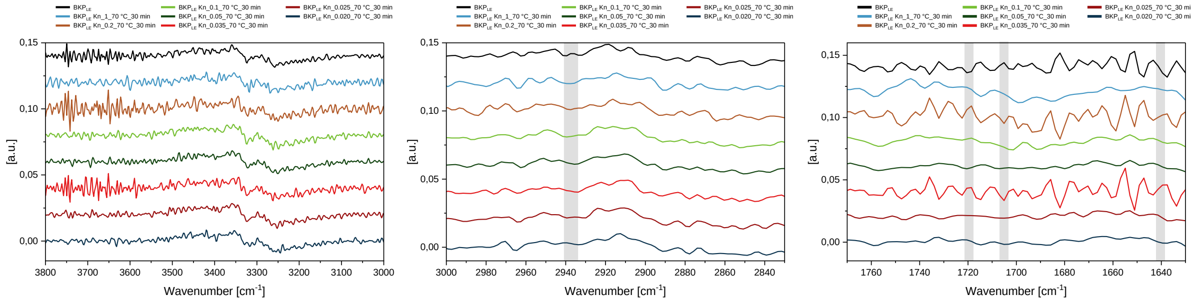

BKP$_{LE}$ Gas - reactions

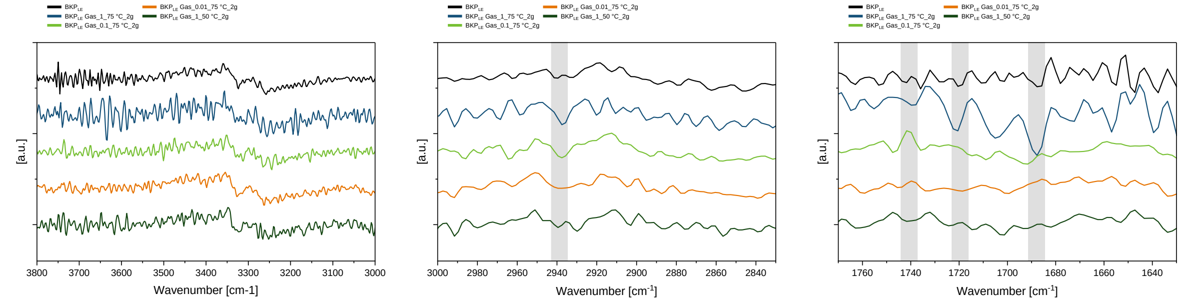

Figure 24. Spectra of the first derivative for the three different modification methods, for different regions, 3800-3000 cm^{-1}, 3000-2830 cm^{-1}, 1790-1630 cm^{-1}. Regions of interest are marked with grey stripes. Top: BKP$_{ND}$ Kn-reaction, Middle: BKP$_{LE}$ Kn-reaction, Bottom: BKP$_{LE}$ Gas.

With regard to the gas phase reactions, a small minimum found in the reference is turned into a larger one, for all reactions. The strongest change is observed for BKP$_{LE}$ Gas_1_75 °C_2g with all other modifications showing smaller minimum values. This indicates that the change in C-H conformation in the case of gas-phase reactions is not only dependent on the molar ratio used during reaction, but also temperature which is seen when comparing BKP$_{LE}$ Gas_1_75 °C_2g to BKP$_{LE}$ Gas_1_50 °C_2g. The first derivative of the carbonyl region, also seen in Figure 24, confirms what has been discussed previously, that different types of reactions seem to promote the formation of different isomers, as illustrated in Figure 19.

5.3 Potentiometric and Polyelectrolyte titration

Titrations were performed based on results from FTIR, as reactions without carbonyl signals or high degree of hornification were excluded. For some reaction conditions, both small and large batches were titrated. The relative charge increase was calculated compared to the references, and as well as the degree of substitution (DS).

In Table 4 a summary is presented, with charges given by equivalences per gram of dry fiber. For BKP_{ND} Kn-reactions, the highest charge increase was seen for BKP_{ND} Kn_1_80 °C_1g, from 0.14 milli-equivalence/g (meq/g) to 0.5 meq/g and a DS-value of 0.027. Calculations are described in section 4.2.2 by Equation 5. BKP_{LE} (no modification) has a lower charge compared to BKP_{ND}, most likely due to the removal of hemicellulose as seen in the carbohydrate analysis. For the BKP_{LE} Kn-reactions, the highest charge increase was seen for BKP_{LE} Kn_1_70 °C_0.5g, closely followed by BKP_{LE} Kn_0.2_70 °C_12g. BKP_{LE} Kn_0.035_70 °C_1g, which showed a weak carbonyl signal, interestingly presented a change increase from 0.085 meq/g to 0.26 meq/g and a DS-value of 0.014.

*Table 4. A summary of the samples titrated separated into different reaction conditions. The selection was done based on FTIR analysis. The number of itaconic groups is calculated based on Equation 5 in section 4.2.2. * 12g reaction, ** 10g reaction.*

Reaction	**NaOH titration (meq/g)**	**Relative charge increase, compared to the respective reference**	**Number of itaconic groups per hydroxyl group on AGU.**
BKP_{ND}	0.14±0.01	1	-
BKP_{ND} Kn_1_80 °C_1g	0.50±0.03	3.6	0.027
BKP_{ND} Kn_0.5_80 °C_0.5g	0.35±0.04 0.32±0.04*	2.5 2.3*	0.019 0.017*
BKP_{LE}	0.085±0.02	1	-
BKP_{LE} Kn_1_70 °C_0.5g	0.65±0.02	7.65	0.035
BKP_{LE} Kn_0.2_70 °C_12g	0.50±0.01	5.9	0.027
BKP_{LE} Kn_0.1_70 °C_60g	0.35±0.01	4.11	0.019
BKP_{LE} Kn_0.035_70 °C_1g	0.26±0.015	3	0.014
BKP_{LE} Gas_1_75 °C_2g	0.38±0.03 0.28±0.03**	4.5 3.3**	0.021 0.015**
BKP_{LE} Gas_0.1_75 °C_2g	0.50±0.03	5.9	0.027
BKP_{LE} Gas_0.01_75 °C_2g	0.18±0.02	2.1	0.010
BKP_{LE} Gas_1_50 °C_2g	0.28±0.05	3.3	0.015

For the gas-phase reactions, BKP_{LE} Gas_0.1_75 °C_2g expressed the highest charge of 0.50 meq/g, surprisingly higher than BKP_{LE} Gas_1_75 °C_2g. Several aspects can give rise to this, most likely the influence of fluffing, drying, and partial pressure of ITA during reaction (Table 2). This also explains the difference between the 2g and 10g batches of gas-phase modification in 1:1 molar ratio at 75 °C.

For polyelectrolyte titration, the larger batches were used as each data point requires approximately 0.5g dry fiber. The titration with polyDADMAC is used to assess surface charges, whilst polyBRENE assesses the total charges of the fibers. This again relates to the assessment of differently available charges present within the fiber structure, fully, partially or buried, as previously explained. Due to the distribution and accessibility of these different charges, not all of them contribute to the final value. In a perfect system, the total charge assessed through polyelectrolyte titration and the titration with NaOH should be the same; however, due to these accessibility differences, tis hardly is the case in real systems.

Further, $^{-}$OH ions are much smaller than polymers and hence penetrate the fiber wall better, detecting more groups. The "inner fiber charge" was calculated by subtracting the surface from the total charge, using values from the polyelectrolyte titrations.

Table 5 summarizes the values from the polyelectrolyte titration in comparison to the titration with NaOH. For all samples the surface and total charge increased compared to the reference. BKP_{LE} Kn_0.1_70 °C_60g and BKP_{LE} Gas_1_75 °C_10g both have the same total charge of 0.128 meq/g, but drastically different surface charges of 0.018 and 0.044, respectively. This indicates that the location of modification differs depending on the method used. Gas-phase may be better at decorating the fiber surface, whilst the kneading reaction of BKP_{LE} seems to penetrate the fibers deeper, likely due to the mechanically aided transport of reagents into the fiber. BKP_{ND} Kn_0.5_80 °C_12g increased in both surface and total charge compared to its reference, with charges being predominantly within the fiber, rather than the surface.

Table 5. Comparison between charges quantified with NaOH titration, polyDADMAC (surface charge) or polyBRENE (total charge). The "inner fiber charge" is calculated by subtracting the surface form the total charge.

Reaction	**NaOH titration (meq/g)**	**Surface charge (meq/g)**	**Total charge (meq/g)**	**Inner fiber charge (meq/g)**
BKP_{ND}	0.14±0.01	0.006	0.029	0.023
BKP_{ND} Kn_0,5_80 °C_12g	0.32±0.04	0.0115	0.108	0.0965
BKP_{LE}	0.085±0.02	0.0124	0.035	0.0226
BKP_{LE} Kn_0,1_70 °C_60g	0.35±0.01	0.0186	0.128	0.1094
BKP_{LE} Gas_1_75 °C_10g	0.28±0.03	0.0439	0.128	0.0841

For the two reference pulps, BKP_{ND} and BKP_{LE}, the inner fiber charge seems to remain the same, whilst the surface charge in BKP_{ND} is approximately half of that for the liquid exchanged BKP, BKP_{LE}. The differences between the different charges are attributed to the removal of hemicelluloses, which alter the supramolecular structure and hence the accessibility, as previously discussed.

5.4 WRV and TBV

The water retention and teabag-values were assessed for the different fibers. The Tea-bag test measures the water between fibers and inside the fiber lumens, whereas WRV quantifies the water retained within the fiber wall (Jayme 1958, Abson and Gilbert 1980). Both the WRV and TBV are often correlated to the surface charge (Table 6) due to the ability of carboxylic acid to form hydrogen bond with water, thereby retaining it. The WRV and TBV are presented alongside the carboxylic acid content determined through titration with NaOH. No clear trend between charge, WRV and TBV can be seen, indicating that confirmational changes upon drying and washing of the fibers overrules the contribution of charge in relation to the water holding capacity of the fibers.

Table 6. WRV and TBV alongside charges determined through titration with NaOH.

Reaction	**NaOH titration (meq/g)**	**WRV (g/g)**	**Teabag (g/g)**
BKP_{ND}	0.14±0.0065	0.98±0.02	30.5±1.5
BKP_{ND} Kn_1_80 °C_1g	0.50±0.03	0.70±0.05	36.0±2.2
BKP_{ND} Kn_0,5_80 °C_0.5g	0.35±0.04	0.84±0.02	42.3±1.7
BKP_{LE}	0.085±0.02	1.09±0.06	42.4±2.2
BKP_{LE} Kn_1_70 °C_0,5g	0.65±0.02	0.89±0.09	46.0±7.4
BKP_{LE} Kn_0,2_70 °C_12g	0.50±0.01	0.75±0.1	32.5±2.3
BKP_{LE} Kn_0,1_70 °C_60g	0.35±0.01	0.81±0.2	28.1±5.8
BKP_{LE} Kn_0,035_70 °C_1g	0.26±0.015	0.83±0.05	37.3±5.9
BKP_{LE} Gas_1_75 °C_2g	0.38±0.03	0.68±0.02	40.5±3.1
BKP_{LE} Gas_0,1_75 °C_2g	0.50±0.03	0.77±0.03	35.4±2.1
BKP_{LE} Gas_0,01_75 °C_2g	0.18±0.02	0.82±0.05	34.5±2.2
BKP_{LE} Gas_1_50 °C_2g	0.28±0.05	0.85±0.07	32.4±3.1

5.5 CP/MAS ^{13}C NMR and PXRD

Both CP/MAS ^{13}C NMR and PXRD can be used to assess the crystallinity of fibers and their composition. NMR may be used to qualitatively assess the morphology of the fibers, whilst PXRD only measures the crystalline parts within the structure. For NMR, Hult et al (2002) described and explained that the most drastic changes in cellulose fiber structures are observed in the C4 region, between 80-92 ppm. For the analysis, the samples were therefore normalized to the 89-ppm signal to visualize changes in the region between 80-92 ppm, Figure 25. All modified samples expressed lower signals compared to the respective references. Further, a higher surface charge is seen to lead to a lower signal in the region between 80 to 86 ppm due to the change in cellulose polymer stacking upon modification.

It should be noted that no signal for the itaconic functionality is visible in the NMR spectra. This is due to two major reasons. Firstly, the DS of the modification is too low to detect, and secondly, the itaconic functionality is much smaller than the rest of the cellulose fibers and is hence likely swallowed in the noise. In some spectra small increases in signal between 120-160 ppm may be observed, however, too small to determine if these are noise or signal.

BKP$_{ND}$ Kn - reactions

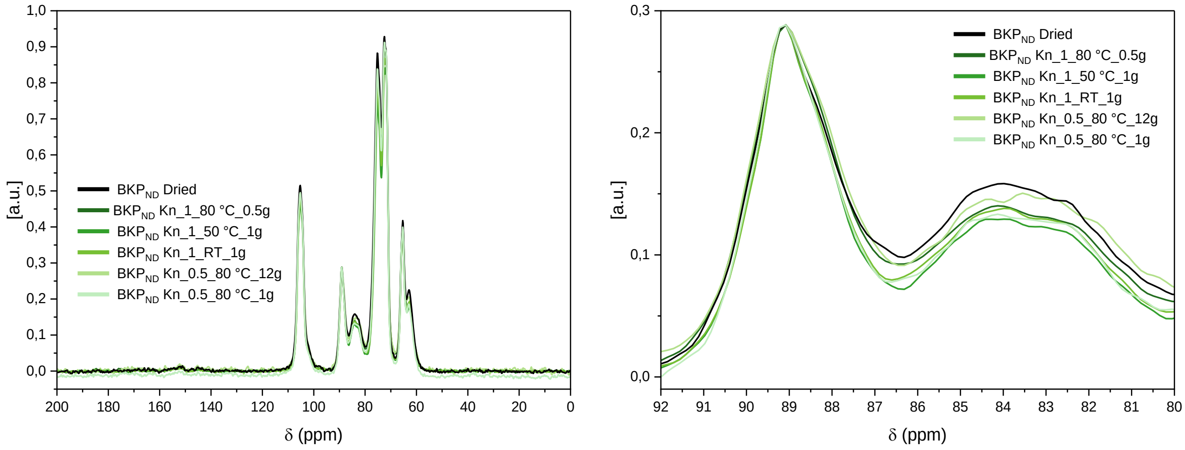

BKP$_{LE}$ Kn - reactions

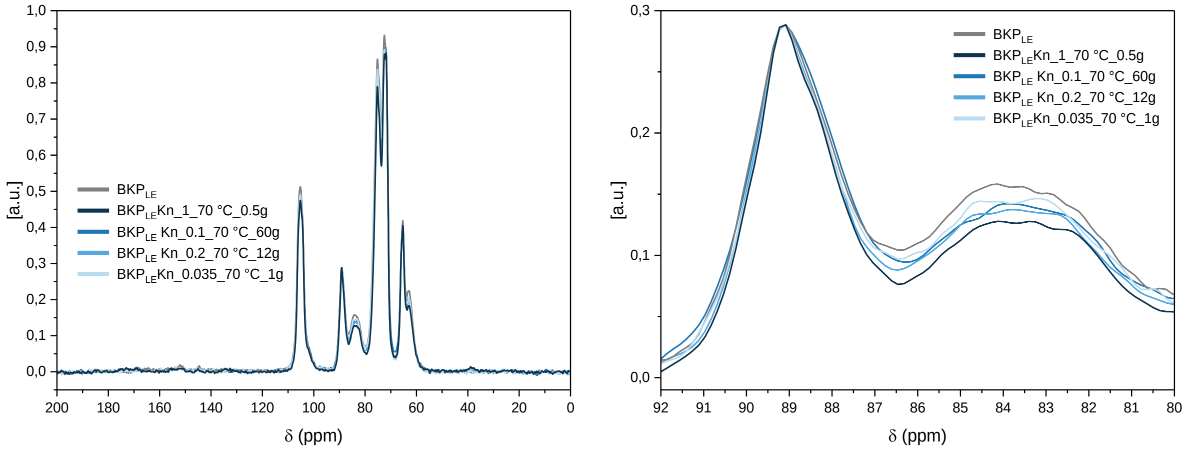

BKP$_{LE}$ Gas - reactions

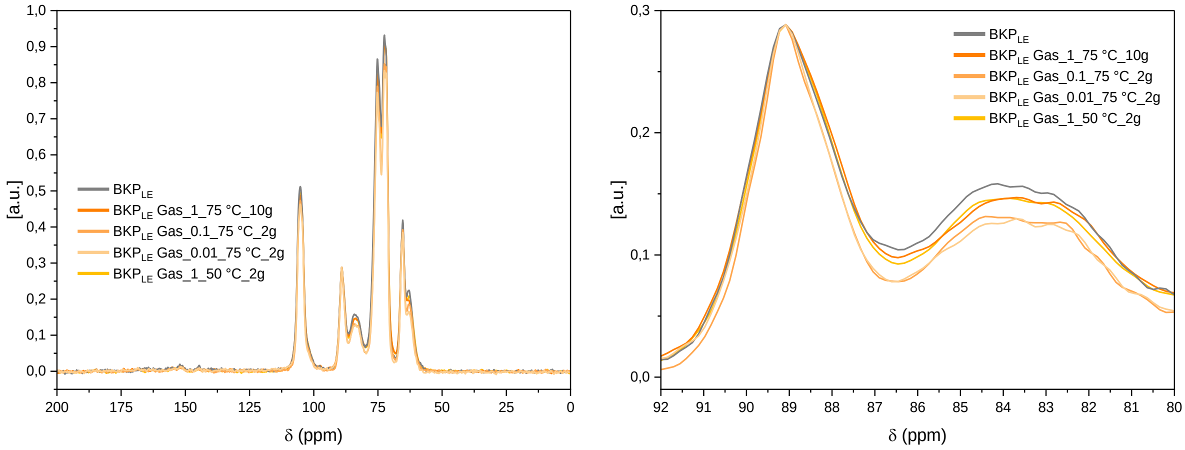

Figure 25. CP/MAS ^{13}C NMR spectra collected for the different reaction conditions. Left: Complete spectra. Right: Magnified to the region between 92 and 80 ppm to visualize structural changes upon derivatization.

PXRD data of the fibers were collected and the average crystallite size calculated based on the Scherrer equation for the (200) plane. As presented in Table 7 no drastic change in average fiber crystallite size is present, indicating that no fiber degradation occurs upon modification. However, this method only investigates the crystalline parts of the fibers, neglecting the amorphous surface polymers where the majority of chemical modification occurs. Small increases may be due to water loss and the incorporation of more polymer chains into the crystal, thereby increasing its average size.

Table 7. Summary of the calculated crystallite sizes with the Scherrer equation for different modifications.

Reaction	**L (nm)**
BKP_{ND}	4.29
BKP_{ND} Kn_1_80 °C_1g	4.45
BKP_{ND} Kn_0.5_80 °C_1g	4.38
BKP_{ND} Kn_0.5_80 °C_12g	4.40
BKP_{LE}	4.37
BKP_{LE} Kn_1_70 °C_0.5g	4.48
BKP_{LE} Kn_0.035_70 °C_1g	4.72
BKP_{LE} Kn_0.2_70 °C_12g	4.60
BKP_{LE} Kn_0.1_70 °C_60g	4.44
BKP_{LE} Gas_1_75 °C_2g	4.29
BKP_{LE} Gas_0.1_75 °C_2g	4.39
BKP_{LE} Gas_0.01_75 °C_2g	4.64
BKP_{LE} Gas_1_50 °C_2g	4.52

5.6 Esterification reactions with MCC

As a control reaction, a kneading reaction was performed using MCC. The reaction was performed to assess the influence of hemi-cellulose and effect of crystallinity on the reactivity of ITA with cellulose. The absence of carbonyl signal for the reaction indicates that no esterification has occurred, and that hemicellulose plays a significant role in the esterification, either through structural effects by creating a more open system or by presenting more sites for modification. Based on WRV/TBV, NMR and PXRD, the structural factor seems the most likely. Further, FTIR comparison between BKP_{LE} and MCC (Figure 26) shows no significant differences, indicating that there is little change in the chemical environment between the two systems.

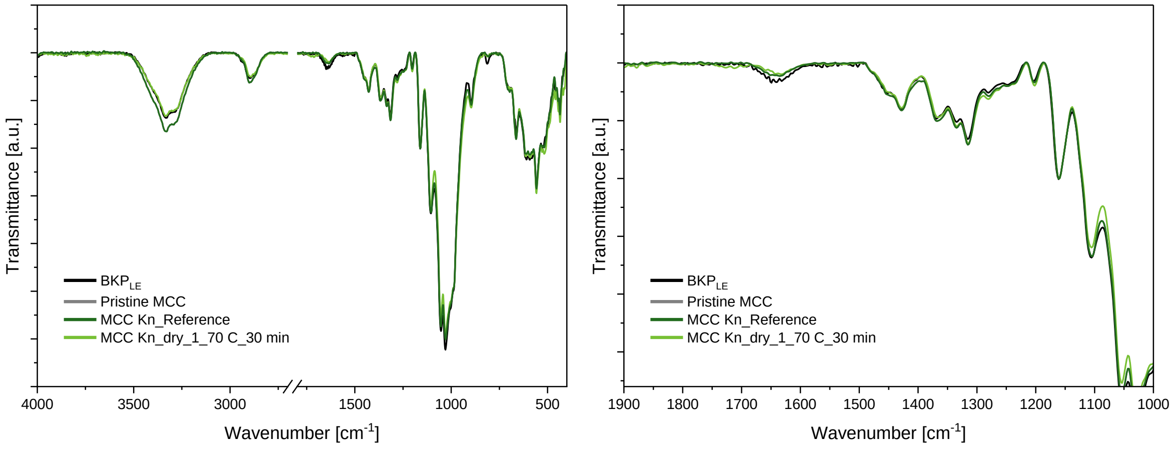

Figure 26. FTIR spectra comparing the chemical composition of MCC with BKP_{LE}.

5.7 Sheet formation of modified and unmodified fibers

To assess the paper formation properties of the modified fibers, sheets were formed in a semi-automated Rapid Köthen apparatus. The formed paper sheets were measured after conditioning at 50 % RH and 23 °C for 24h. The curve of tensile stress plotted against tensile strain is given in Figure 27. BKP$_{LE}$ Kn_0.1_70 °C_60g is visibly weaker than the reference paper, likely due to the incorporation of itaconic acid groups which inhibit proper fiber interaction due to repellent forces between the charged groups, leading to friction in the paper. Further differences were measured for the formed sheets such as roughness where BKP$_{LE}$ Kn_0.1_70 °C_60 measured to be higher, like the paper thickness.

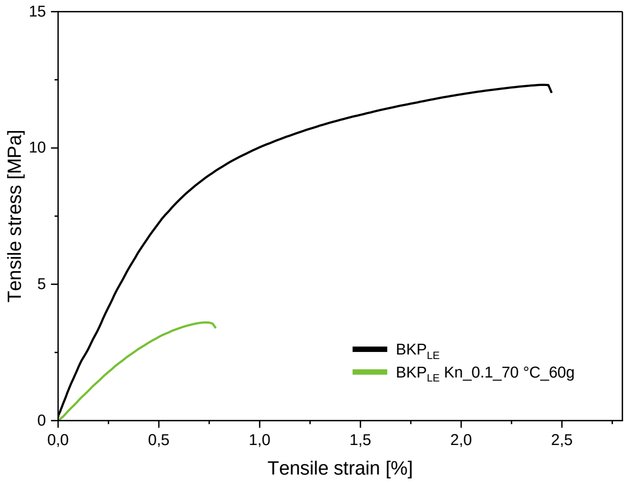

Figure 27. Tensile test curve for BKP$_{LE}$ and BKP$_{LE}$ Kn_0,1_70 °C_60g.

Table 8 summarizes the other material properties measured, such as sheet thickness and grammage, needed for the assessment of tensile strength and stress. The roughness of the two different sheets was also measured. BKP$_{LE}$ Kn_0.1_70 °C_60 presented a higher degree of roughness and thickness compared to the reference sheet, consistent with the lower density packing of the fibers during sheet formation.

Table 8. Data collected for formed sheets, BKP$_{LE}$ and BKPLE Kn_0.1_70 °C_60g.

	Reference sheet	**BKP$_{LE}$ Kn_0.1_70 °C_60g**
Grammage (g/m^2)	61	57
Thickness (mm)	0.1126	0.1551
E (elongation)	2.5%	0.8%
σ_T^W (kNm/kg)	31	10
σ_T^b (kN/m)	1.9	0.5
Rougness, upside (ml/min)	702	1408
Rougness, downside (ml/min)	750	1598

The material properties of the sheet made exclusively from BKP-itaconate do not show excellent mechanical properties in terms of strength, but may, in combination with pristine BKP, express better mechanical strength whilst also exhibiting excellent chemical properties for wet strength through cross-linking or similar.

CHAPTER 6
RESULTS – CNC SUSPENSIONS AND FILMS

This chapter summarizes the findings from Paper II and III, relating to CNC studies. Additional results are added for measurements conducted at beamline B23, Diamond Light source, UK, denoted as B23-MMP, concerning CNC-light interactions for studies on aggregation, structure and assembly.

6.1 Chemical modification of CNC

The chemical modification of CNC was assessed using ATR-FTIR as the primary method. Changes observed in the region around 810 cm^{-1} are commonly utilized to monitor variations in the vibrational frequencies of sulfate half esters. Figure 28 presents the FTIR of the CNCs used in *Paper II* (change in counter ions) and *Paper III* (tuning with Az-salts). In *Paper II*, small changes in the 810 cm^{-1} frequency region are detected for all samples, due to different counter ions.

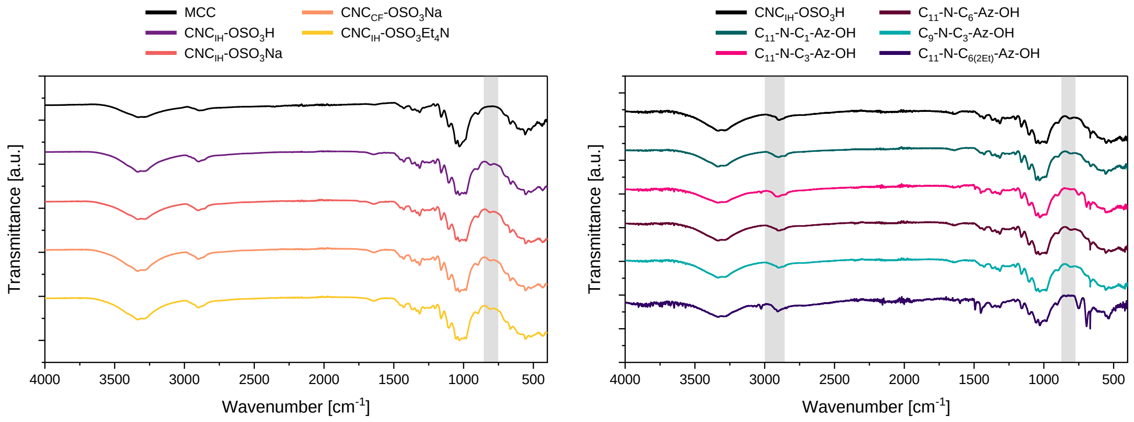

Figure 28. Left: FTIR spectra of different CNCs with different counter ions, paper II. Right: The FTIR of Az-salt modified CNC films. In both cases the signal of the sulfate groups occurs around 810 cm^{-1} and shifts slightly depending on the counter ion/covalent modification of the film. Data taken and plotted from Paper II and III, respectively.

In *Paper III* the properties of CNC were tuned by conjugating Az-salts to the sulfate group of CNC. Five different modifications were made, using C_{11}-N-C_1-Az-OH, C_{11}-N-C_3-Az-OH, C_{11}-N-C_6-Az-OH, C_9-N-C_3-Az-OH and C_{11}-N-$C_{6(2Et)}$-Az-OH Az-linkers. For all samples, a small shift from 814 to 808 cm^{-1} in the C–O–S region detected, indicating of a successful sulfate modification. The C-H region between approximately 3000 cm^{-1} to 2850 cm^{-1} is also studied due to the incorporation of alkyl chains. All six samples gave the expected signal for the presence of cellulose with a contribution from the grafted propyl-2-hydroxy-dialkyl chains.

A similar trend to what is seen in *Paper II* is seen for the B23-MMP series, presented in Figure 29. The characteristic cellulose signals are present alongside the signal for the sulfate half tester at around 810 cm^{-1}. Again, a small change is detected for the change in counter ion.

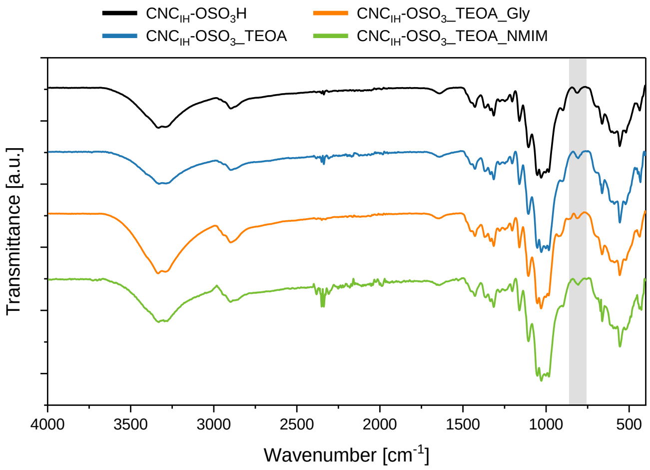

Figure 29. Full FTIR spectra of CNC films studied for B23-MMP project.

6.2 Optical studies of CNC films

To assess the influence of counterions of the CNC suspension on their aggregation, POM images were made in *Paper II*. As stated in Chapter 4, the samples were prepared with or without sonication (Son) prior to casting, as well as drying at ambient or elevated temperature, alternatively in an evacuated dessicator (Vac). Two types of CNC were used, either in-house produces or purchased CNC, CNC$_{IH}$ and CNC$_{CF}$ respectively.

CNC$_{IH}$-OSO$_3^-$X$^+$ films prepared without sonication all display a mosaic of grains with very small needle-shaped ~0.1–2 µm^2 cross-sections, indicating independent light scattering (Figure 30) For the CNC$_{IH}$-OSO$_3$H sample, dark areas are present which appear to be birefringent, meaning a void rather than light extinction due to isotropy.

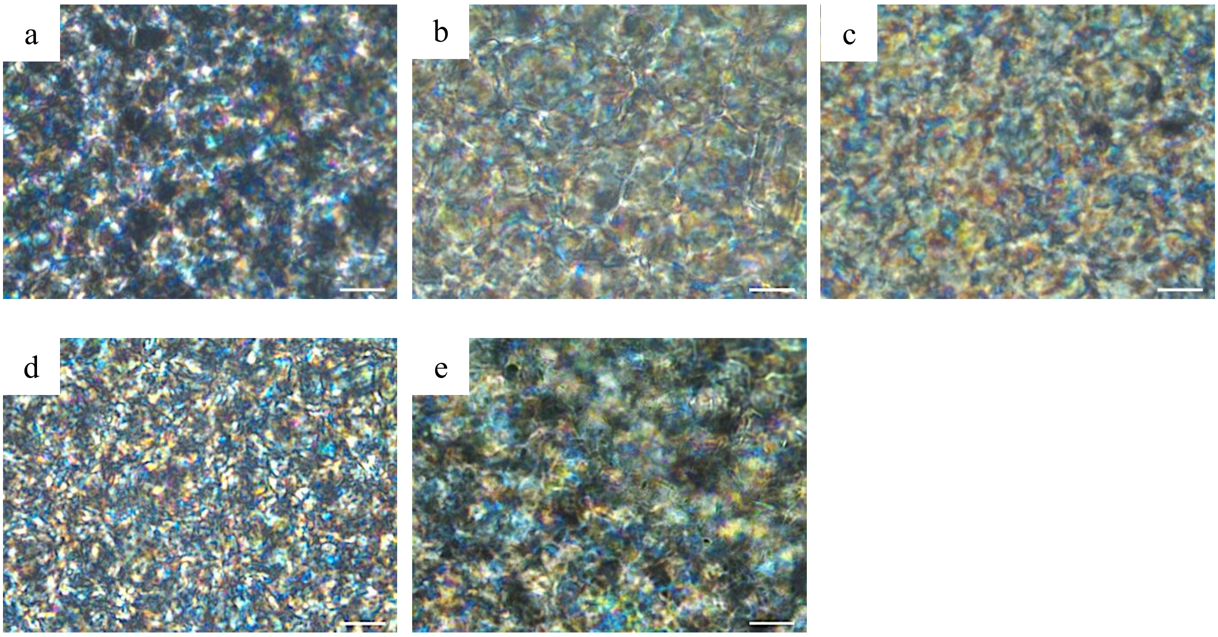

Figure 30. POM micrograph images of CNC-OSO$_3^-$ -X$^+$ without sonication. a) H+, b) H+ 45, c) H+ Vac, d) Na+, e) Na+ 45. The scale bars are 5 µm. Taken from Paper II.

CNC_{IH}-$OSO_3^-X^+$ and CNC_{CF}-$OSO_3^-X^+$ films prepared with sonication formed transparent films without apparent long-range order are presented in Figure 31, likely due to the breaking of aggregates during sonication leading to closer packing and alignment of particles facilitated through comparably slow aggregation during drying. Interestingly, sonicated CNC_{CF}-OSO_3Na presented a multi-domain helicoidal long-range order in near-transparent films.

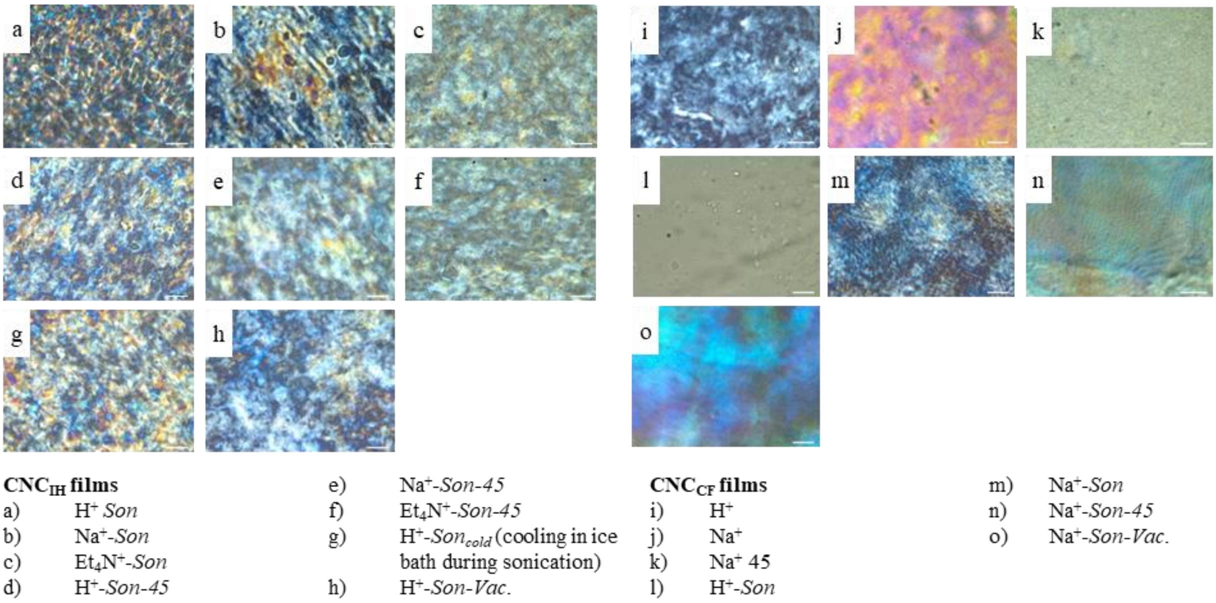

Figure 31. POM images of left: Sonicated CNC_{IH}-$OSO_3^-X^+$ *films prepared with different counterions and drying conditions. Right:* CNC_{CF}-$OSO_3^-X^+$ *films. Note the fingerprint patterns in the sonicated* Na^+ *counterion films in e-f, indicative of cholesteric structure. Scale bas rare set to 5 µm. Taken from Paper II.*

The UV-Vis analysis also showed differences between the samples, further confirming that sample preparation, i.e. sonication has strong effects on the alignment of CNC crystals, as previously discussed by Vignolini et al. Sonicated samples presented as more transparent films, also attenuating less than half of the light of samples prepared without sonication at wavelengths above 325 nm. Films without specific fingerprints/structures presented a broad light attenuation likely due to scattering of light, rather than absorption or transmission.

6.3 Materials properties of CNC suspension and films

The materials properties of CNC films from *Paper II* and *III* explained in this section. TGA and DLS were used in both papers, whilst wettability and mechanical strength were explored exclusively in *Paper II*. *Paper III* explored the rheological properties of CNC suspension.

6.3.1 TGA

TGA was used in both *Paper II* and *III* for characterization of CNC films (Figure 32). In *Paper II* the films were studied on the effect of counter ions, whilst *Paper III* assessed the influence of covalent conjugation to Az-salts. In *Paper II*, MCC was used as an additional reference.

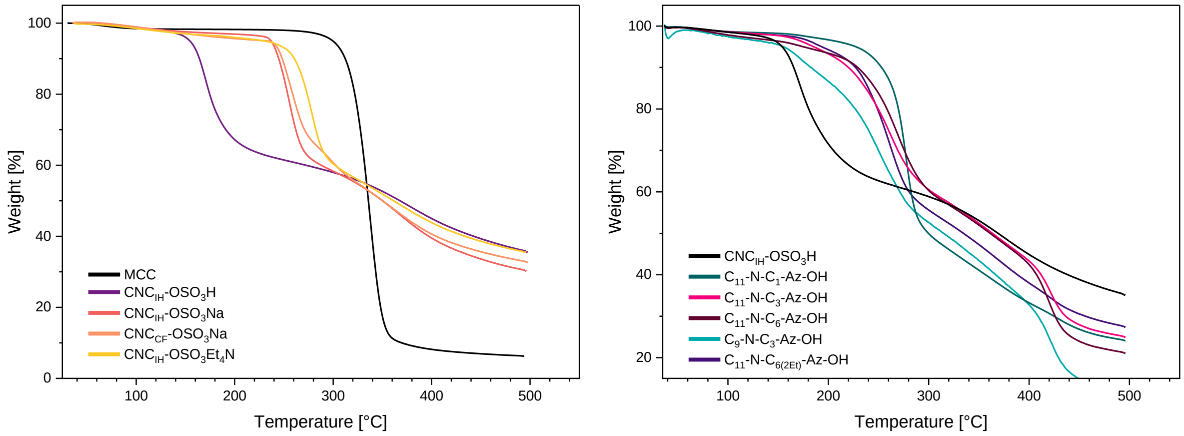

Figure 32. TGA analysis of modified CNC films with counter ions (left), or through conjugation to Az-salts (right). Data taken and plotted from Paper II and III, respectively.

In *Paper II*, the decomposition temperature is reduced from 338 °C in MCC to 174 °C in CNC$_{IH}$-OSO$_3$H films because of the introduction of sulfate ester groups (C-O-SO$_3$H). The auto-catalyzed desulfation, catalyzed by the acidic proton in the -OSO$_3$H group, is visible in the graph, followed by loss of hard-bound water and de-polymerization. For CNCs with Na$^+$ and Et$_4$N$^+$ counterions the degradation of the samples is retarded, with a decomposition temperature between 255–278 °C, due to the inhibition of auto-desulfation. Similar trends are visible for the Az-salt modified CNCs in *Paper III* where the degradation temperature is shifted from 145 °C to 185 °C for pristine to modified CNC.

6.3.2 DLS

In *Paper II*, studying the effects of counterions and suspension preparation and drying, DLS was used to assess the Z-potential and hydrodynamic diameter of the CNC particles. It should be stated that DLS is not strictly applicable to anisotropic particles, however it is widely used as a semi-quantitative analysis of particle size and is a representation of aggregate/cluster size rather than individual CNCs.

All CNC samples show excellent dispersibility in DI water with ζ values>−30 mV and no significant difference was seen in zeta potential between suspensions of different counterions or sonicated versus non-sonicated suspensions. The hydrodynamic diameter of CNC$_{IH}$-OSO$_3$H and CNC$_{IH}$-OSO$_3$Na changed from 6910 ± 983 and 8000 ± 1000 nm to 77 ± 2.31 nm and 89 ± 3.8 nm respectively after sonication, due to clusters of CNCs being broken up after sonication. All suspensions were stable without any visible sedimentation during storage over months (in line with the low ζ values), indicating the formation of lower-density clusters rather than dense aggregates.

DLS was also used in *Paper III*, again showing an average zeta potential close to stable colloidal suspensions for all CNC systems in the presence of NaCl (modified and pristine), with values of >30 mV, as seen in *Paper II*.

6.3.3 Wettability and mechanical properties

Paper II investigated the mechanical properties of CNC films alongside wettability and water stability. Specifically, tensile strength, σ (MPa), and elongation break, ε (%), was studied and correlated to crystallinity index collected from PXRD data, as well as swelling and contact angle (Table 9). In general, sonication increased the tensile strength across all counter ions. Films containing Na$^+$ as counter ion expressed more flexibility in comparison to H$^+$, likely due to the size of the ion. The use of Et$_4$N$^+$ made the films elongate better, likely due to other hydrogen bond interactions between the surface cellulose units and the four ethyl groups.

Table 9. Comparison between mechanical properties of CNC films with swelling/wettability and crystallinity.

CNC film	**σ (MPa)**	**ε (%)**	**CI (%)**	**Swelling (%)**	**Contact angle**
CNC_{CF}-OSO_3H	39.7 (3.1)	1.9 (0.6)	95.6	Unstable	60.5°
CNC_{CF}-OSO_3H *Son*	54.6 (2.8)	2.4 (0.2)	96.2	200% (1 hr)	86.1°
CNC_{CF}-OSO_3Na	41.6 (3.3)	2.7 (0.5)	96	Unstable	42.3°
CNC_{CF}-OSO_3Na *Son*	65.4 (4.1)	2.1 (0.5)	96.5	190% (5 mins)	63.2°
CNC_{IH}-OSO_3H	28.2 (2.8)	1 (0.1)	96.2	Unstable	62°
CNC_{IH}-OSO_3H *Son*	65 (3.5)	2.8 (0.2)	97	190% (5 mins)	72°
CNC_{IH}-OSO_3Na	39.6 (3.8)	1.6 (0.1)	96.7	Unstable	48°
CNC_{IH}-OSO_3Na *Son*	59.8 (3)	2.2 (0.5)	97	175% (5 mins)	70°
CNC_{IH}-OSO_3Et_4N *Son*	70.5 (3.7)	2.5 (0.6)	96.8	Unstable	72°
CNC_{IH}-OSO_3Na *Son-45*	61.4 (3)	2.2 (0.5)	97.5	200% (5 mins)	69°
CNC_{IH}-OSO_3Na *Son-Vac*	70 (4.1)	2.3 (0.8)	97.9	180% (5 mins)	75°
CNC_{CF}-OSO_3Na *Son-45*	63.25 (4)	1.5 (0.9)	95	-	-
CNC_{CF}-OSO_3Na *Son-Vac*	77.6 (3.8)	1.7 (0.4)	97	-	-

Results from wetting (swelling) test conclude that sonication drastically increases the water stability of the films, due to the slow aggregation with small voids, compared to non-sonicated samples. The contact angle (surface wettability) also increased for all sonicated samples. Further, samples having H^+ were more water resistant compared to Na^+ as counterion, possibly because of the inter-crystal distance increasing with larger ions. The crystallinity index of the different samples, comparing the (200) reflection intensity with the amorphous part shows high crystallinities for all samples.

6.3.4 Rheological assessment of CNC suspensions

Paper III was conducted in collaboration to understand the influence of Az-salts conjugation on CNC aggregation. It was shown that the conjugation of Az-salt drastically impacts the viscosity and dynamic moduli of the suspensions, specifically for 1.5 wt.%, where unmodified CNC lies below the gel point, whereas modified suspensions are rheological (isotropic) gels. Further, longer linkers generally show to have a higher impact to linear viscoelastic properties of the suspensions. From a chemical point of view, this is plausible due to steric hindrance induced by the side chains as well as their hydrophobic interactions, thereby influencing the organization of the CNC crystals. Alongside linear Az-salts, one branched salt was used for the conjugation to further explore the size and distribution influences on the interactions.

Other projects in collaboration with other research groups (not included in this thesis) have investigated the space occupancy of side chains in relation to CNC aggregation, by combining rheological measurements and modelling (Wojno, Sonker et al. 2024). It was concluded that linker topology heavily influences the rheological and optical properties, and that the conjugation of Az-salts to the CNC therefore enables great tunability for creating advanced materials. (Wojno 2023, Wojno, Sonker et al. 2024)

6.4 B23-MMP

The previously described findings related to CNC provided the foundation for a subsequent study employing MMP analysis. In Figure 33 the plots from the MMP analysis of four samples, pristine CNC-OSO$_3$H, CNC-OSO$_3$_TEOA, CNC-OSO$_3$_TEOA_Gly, and CNC-OSO$_3$_TEOA_NMIM, are presented. For each film, the surface was mapped, generating a MMP matrix, from which parameters such as circular dichroism (CD), circular birefringence (CB), absorbance, linear dichroism (LD), linear birefringence (LB), G-factor, LD', LB', and the dissymmetry index (DI) were derived. While the MMP matrix alone offers insight into differences in molecular aggregation and alignment across the samples, further analysis of the individual components allows for a more comprehensive understanding

For the CD plot, that is the interaction between left or right-handed light, the reference sample seems to predominantly be ordered to absorb into left-handed light (red), with some right-handed-absorbing regions present (blue spots). In all films with additives (TEOA, TEOA_Gly, and TEOA_NMIM), almost no right-handed-absorbing structure is present, already indicating that the additives influence the ordering of the CNC crystals.

The LD signals arise from the difference in absorption between parallel and perpendicular light to the orientation axis in CNC and can provide information of the transition dipole moment in the molecule. In the reference sample, the LD signal seems to be dominated by a parallel alignment, which is slightly disordered by the addition of TEOA and TEOA_Gly, whilst being more ordered by the addition of TEOA_NMIM. Similarely, significant differences can be observed in circlar birefringence (CB), where the addition of NMIM again introduces high degrees of order.

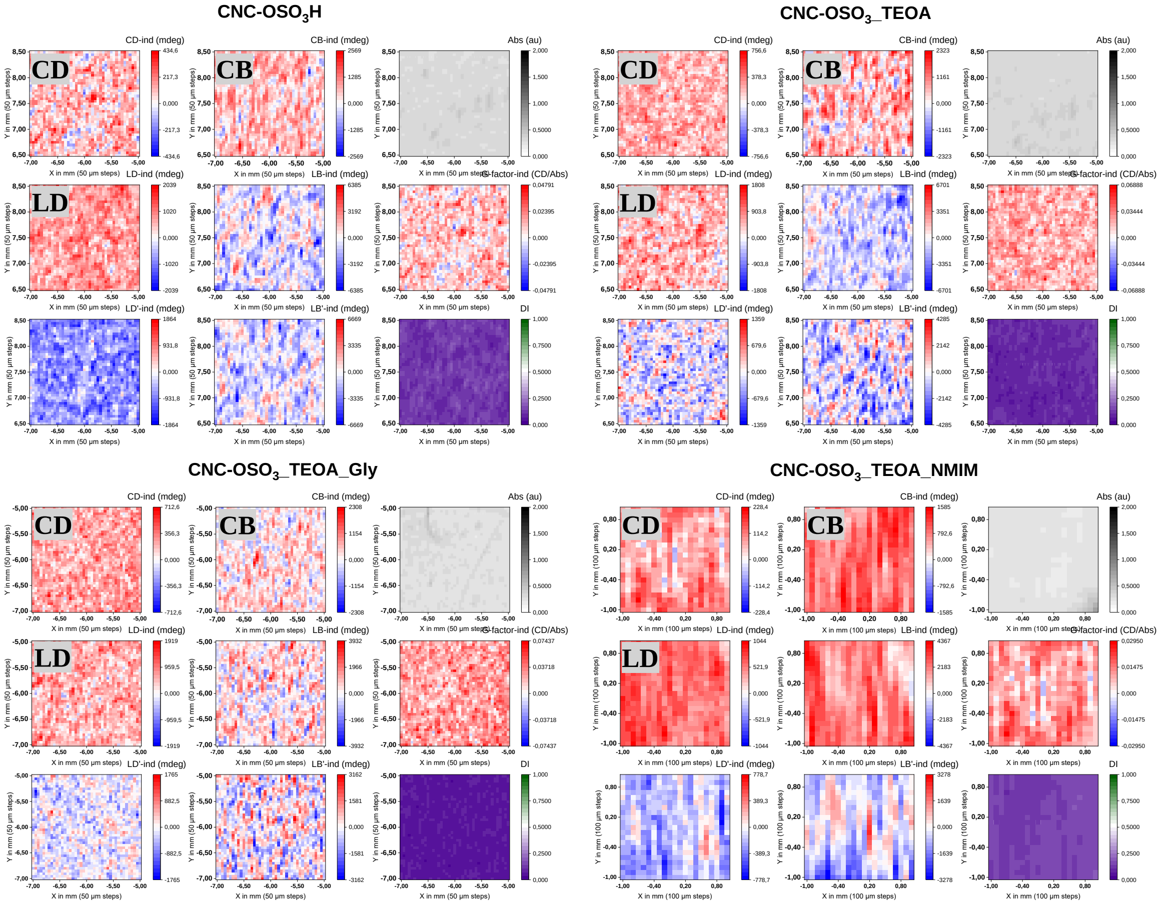

Figure 33. Summary of components measured of the different films.

Combining the B23-MMP plots with POM and SEM images, the possible alignments may be elucidated as illustrated for the CNC-OSO$_3$_TEOA film, Figure 34. The POM image presents no sign of birefringence, indicating the lack of a chiral nematic phase. Similarly, the cross section of the films, recorded with SEM, also showed no distinct chiral nematic structures, but instead appears to be only nematic or possibly smectic.

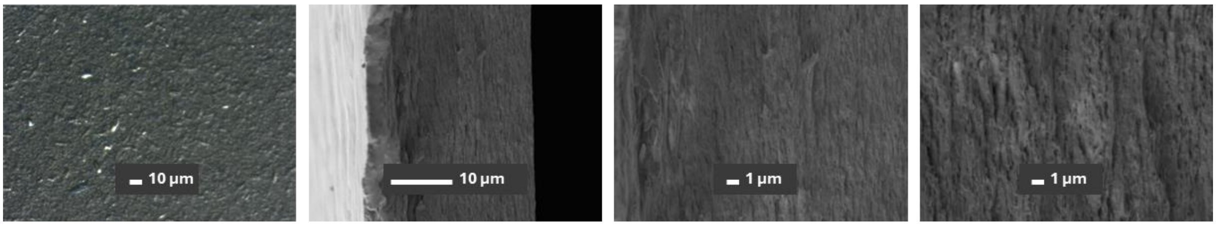

Figure 34.CNC-OSO$_3$_TEOA film with left being the POM image, followed by three SEM images. No change in color is observed from the POM image, indicating to the chiral nematic phase in the film.

Comparing this to the finding from *Paper II*, it seems that the type of counterion attached to the sulfate group on the CNC heavily influences their extent of hindering the chiral nematic aggregation. The TEOA, being much larger in size compared to H^+ or Na^+ and Et_4N^+, seems to by itself restructure the cellulose whilst the effects are increased with the addition of Gly and NMIM. This is most likely due to the size and spatial occupancy of the ions, acting either as a slipping-layer or as an anchoring/crosslinking point. An illustration of the different systems is presented in Figure 35.

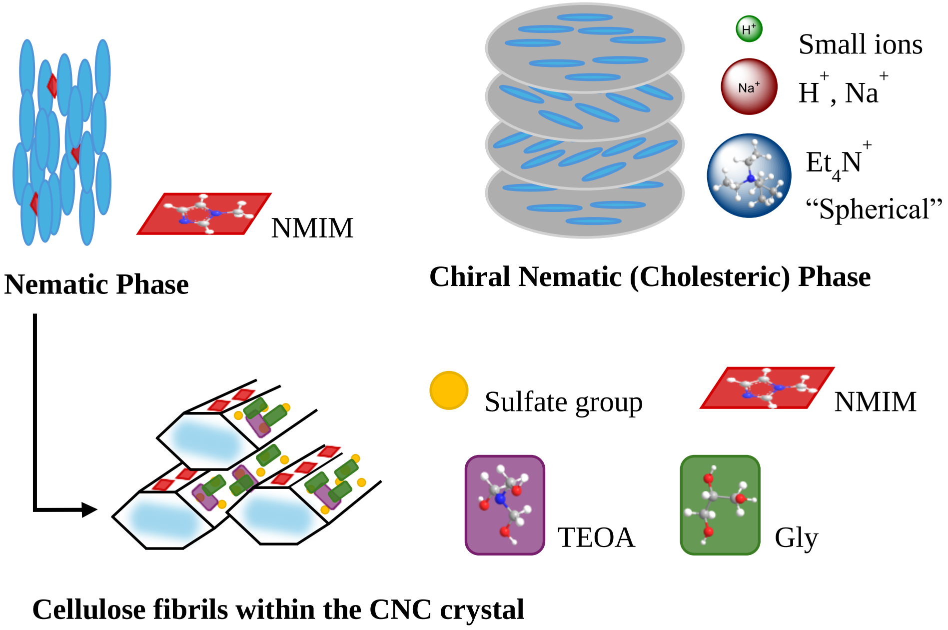

Figure 35. Illustraion of the ordering of CNCs into Nematic or Chiral Nematic structures, depending on the additive.

As illustrated in the figure, based on experimental findings, the different additives interplay in different ways with the sulfonated CNC crystals. Small ions, such as H^+ and Na^+ do not disrupt the formation of the chiral nematic structure, as also seen in POM images. The addition of Et_4N^+ seems to disrupt this alignment somewhat, likely due to its size. However, looking at its molecular structure, it may be envisioned as a large semi-spherical particle, likely to interact in a similar way to H^+ and Na^+.

The nonsymmetrical amines, such as TEOA, coordinate to the sulfate-ester through its nitrogen atom, allowed due to its conformation and pointing of the alkyl groups. This leads to the formation of a more nematic phase, compared to pristine CNC. Gly, as added together with TEOA and not itself being charged, is instead thought of as interacting with the hydroxyl groups on the cellulose fibrils trough hydrogen bonding, creating links along the sides of them and interlocking the system. I combination with TEOA, the amine blocks some of this interaction by coordinating to the sulfate with its nitrogen, whilst the hydroxyl groups of its alcohol chain instead interact with the glycerol. As sulfate groups occur on more than one side of the crystal, with the TEOA_Gly complex between them, it becomes more of a dynamic layer also disrupting the formation of the chiral nematic phase.

Based on the LD signal of the TEOA_NMIM film, and the planar structure of NMIM it is thought to interact in between the cellulose fibrils, along the (200) plane, acting as a slipping layer, forming a nematic structure.

CHAPTER 7
CONCLUDING REMARKS

This thesis consisted of two topics, fibers and CNC, both concerning their chemical modification and its influence on the supramolecular structure of the materials. The first part aimed to summarize the finding in Manuscript I, the esterification of BKP with itaconic anhydride, gaining BKP-itaconate. The second part summarized findings in Paper II, the modification of CNC with counter ions or Azetidinium salts, alongside additional information from the B23-MMP experiments.

7.1 Conclusion

From *Manuscript I,* fiber modification, it was shown that the modification of BKP is possible with ITA through three different methods. Although the carboxylic acid charge is the same for some of the reactions, their FTIR spectra exposes differences in the chemical bonding and confirmation of fibers and present possible isomerization of itaconic acid into citraconic or mesaconic acid. Neither the WRV or teabag values showed a clear correlation between water-holding capacity and fiber charge. This together with the NMR and XRD studies concludes that confirmational changes of the cellulose fibers “overrule” the charge in terms of material properties, such as water holding. Further, no degradation of the fiber was observed, meaning that most of the mechanical properties of the fiber most likely remain intact, although the mechanical testing showed significant decrease in mechanical strength, possibly due to friction between the fibers. Nonetheless, the tensile test of the paper only measures the bulk property, not the strength of the individual fiber. The polyelectrolyte titrations showed different charge distribution amongst the different reactions (gas or kneading), which also may be due to confirmational changes during the fiber processing.

In *Paper II,* the assembly and drying of CNC in suspension to films was investigated, specifically on the effects of counter ions and sonication. It was concluded that the sonication of suspensions prior to film casting strongly influenced the optical mechanical properties such as wetting and tensile strength as well as the optical properties of the CNC films, due to differences in packing and organization. *Paper III* explored the conjugation of Az-salts, in particular, rheological measurements were conducted to understand the effects of the size and branching of side chains, showing that the addition of such strongly influenced the gel point of CNC suspensions, behaving as isotopic gels at 1.5 and 3 wt.%. This behavior was concluded to be due to chin mobility and branch-to-branch topologies.

From measurements conducted at Diamond Light Source, B23-MMP, clear differences in CD, LD and CB signals are seen for the different modified samples, with the CNC-OSO_3H_TEOA_NMIM film expressing the most directional order compared to CNC-OSO_3H_TEOA, CNC-OSO_3H_TEOA_Gly, and CNC-OSO_3H reference film. As many of these results are preliminary, they are not discussed in detail in this thesis but will be explored further in the forthcoming PhD thesis.

7.2 Future Research

As future research interest serval things come to mind. Firstly, this thesis has not discussed the possibility of polymerizing H_2IA onto the fiber surface or even within the fibril. Secondly, to combine the functionalization of CNC with the functionalization of BKP-Itaconate, introducing Az-salts functionalities for better wet-strength abilities. Similarly, it would be interesting to investigate the formation of papers with different degrees of modification present and measure the effect of the different modifications (kneading or gas-phase) on the paper formation and mechanical properties.

To connect the optical measurements of CNC-films to fiber-technology, the investigation of fibers at the beamline B23-Diamon Light Source would be insightful to understand the effect of modification of crystallinity and packing, especially for the S2 layers in the fiber wall. CNC, with different additives, will continue to be investigated, as well as their forced alignment in magnetic fields, for an even deeper understanding and formation of innovative and sustainable materials.

ACKNOWLEDGEMENTS

Wallenberg Wood Science Center is acknowledged for their funding to conduct this research.

Firstly, I would like to express my gratitude to my fantastic supervisor, Gunnar Westman, with whom research never stops being interesting and adventurous!

I would also like to thank my two co-supervisors, Kent Malmgren (SCA) and Tomas Larsson (KTH). Thank you, Kent, for making my weeks is Sundvall fun and exciting, and to Tomas for keeping me alert and on my toes. I think I remembered to refer to tings as “signals”, not “peaks”.

I would also like to thank my examiner Jerker for insightful conversations, not only about science, and to Diana Bernin and her group for helping me run ssNMR samples, thank you!

To the 9th floor and its people, for making everyone feel welcome!

And lastly, to all my friends and family (especially Johan) for their everlasting support during the first half of this journey!

References

Abson, D. and R. D. Gilbert (1980). "Observations on water retention values. ." *Tappi*, 63(9), 146.

Agarwal, U. P., S. A. Ralph, C. Baez, R. S. Reiner and S. P. Verrill (2017). "Effect of sample moisture content on XRD-estimated cellulose crystallinity index and crystallite size." *Cellulose*, 24(5), 1971-1984.

Alder, C. M., J. D. Hayler, R. K. Henderson, A. M. Redman, L. Shukla, L. E. Shuster and H. F. Sneddon (2016). "Updating and further expanding GSK's solvent sustainability guide." *Green Chemistry*, 18(13), 3879-3890.

Aziz, T., A. Farid, F. Haq, M. Kiran, A. Ullah, K. C. Zhang, C. Li, S. Ghazanfar, H. Y. Sun, R. Ullah, A. Ali, M. Muzammal, M. Shah, N. Akhtar, S. Selim, N. Hagagy, M. Samy and S. K. Al Jaouni (2022). "A Review on the Modification of Cellulose and Its Applications." *Polymers*, 14(15).

Beatson, R. P. (1992). *Determination of Sulfonate Groups and Total Sulfur. Methods in Lignin Chemistry*. S. Y. Lin and C. W. Dence. Berlin, Heidelberg, Springer Berlin Heidelberg, 473-484.

Borjesson, M., G. Richardson and G. Westman (2015). "UV Radiation of Cellulose Fibers and Acrylic Acid Modified Cellulose Fibers for Improved Stiffness in Paper." *Bioresources*, 10(2), 3056-3069.

Botková, M., S. Suty, M. Jablonsky, L. Kucerkova and M. Vrška (2013). "Monitoring of kraft pulps swelling in water." *Cellulose Chemistry and Technology*, 47, 95-102.

Chu, G. (2024). "Controlled Self-Assembly of Cellulose Nanocrystal as Custom-Tailored Photonics and Complex Soft Matter." *Accounts of Materials Research*, 5(11), 1388-1400.

Cortes Ruiz, M. F., J. Martin, L. Marcos Celada, P. Olsén and L. Wågberg (2025). "Strategic functionalization of wood fibers for the circular design of fiber-reinforced hydrogel composites." *Cell Reports Physical Science*, 6(3), 102455.

Daicho, K., T. Saito, S. Fujisawa and A. Isogai (2018). "The Crystallinity of Nanocellulose: Dispersion-Induced Disordering of the Grain Boundary in Biologically Structured Cellulose." *ACS Applied Nano Materials*, 1(10), 5774-5785.

David, G., N. Gontard, D. Guerin, L. Heux, J. Lecomte, S. Molina-Boisseau and H. Angellier-Coussy (2019). "Exploring the potential of gas-phase esterification to hydrophobize the surface of micrometric cellulose particles." *European Polymer Journal*, 115, 138-146.

Dong, X. M. and D. G. Gray (1997). "Effect of Counterions on Ordered Phase Formation in Suspensions of Charged Rodlike Cellulose Crystallites." *Langmuir*, 13(8), 2404-2409.

Dong, X. M., T. Kimura, J.-F. Revol and D. G. Gray (1996). "Effects of Ionic Strength on the Isotropic−Chiral Nematic Phase Transition of Suspensions of Cellulose Crystallites." *Langmuir*, 12(8), 2076-2082.

Dumanli, A. G., H. M. van der Kooij, G. Kamita, E. Reisner, J. J. Baumberg, U. Steiner and S. Vignolini (2014). "Digital Color in Cellulose Nanocrystal Films." *ACS Applied Materials & Interfaces*, 6(15), 12302-12306.

Ek, M., G. Gellerstedt and G. Henriksson (2007). *Ljungberg Textbook, Volume 1 Wood Chemistry and Wood Biotechnology*. Stockholm, Sweden, KTH.

El Seoud, O. A., L. C. Fidale, N. Ruiz, M. L. O. D'Almeida and E. Frollini (2008). "Cellulose swelling by protic solvents: which properties of the biopolymer and the solvent matter?" *Cellulose*, 15(3), 371-392.

Eronen, P., M. Österberg, S. Heikkinen, M. Tenkanen and J. Laine (2011). "Interactions of structurally different hemicelluloses with nanofibrillar cellulose." *Carbohydrate Polymers*, 86(3), 1281-1290.

Fernandes, A., L. Cruz-Lopes, B. Esteves and D. Evtuguin (2023) "Nanotechnology Applied to Cellulosic Materials." *Materials*, 16(8), 3104.

Fernández-Santos, J., C. Valls, O. Cusola and M. B. Roncero (2021). "Improving Filmogenic and Barrier Properties of Nanocellulose Films by Addition of Biodegradable Plasticizers." *ACS Sustainable Chemistry & Engineering* 9(29), 9647-9660.

Francolini, I., L. Galantini, F. Rea, C. Di Cosimo and P. Di Cosimo (2023) "Polymeric Wet-Strength Agents in the Paper Industry: An Overview of Mechanisms and Current Challenges." *International Journal of Molecular Sciences*, 24(11), 9268.

French, A. D. and M. Santiago Cintrón (2013). "Cellulose polymorphy, crystallite size, and the Segal Crystallinity Index." *Cellulose*, 20(1), 583-588.

Frka-Petesic, B., T. G. Parton, C. Honorato-Rios, A. Narkevicius, K. Ballu, Q. Shen, Z. Lu, Y. Ogawa, J. S. Haataja, B. E. Droguet, R. M. Parker and S. Vignolini (2023). "Structural Color from Cellulose Nanocrystals or Chitin Nanocrystals: Self-Assembly, Optics, and Applications." *Chemical Reviews*, 123(23), 12595-12756.

Han, X., P. Chen, L. Li, Y. Nishiyama and X. Yang (2023). "Planar and uniplanar orientation in nanocellulose films: interpretation of 2D diffraction patterns step-by-step." *Cellulose*, 30(13), 8151-8159.

Hribernik, S., K. Stana Kleinschek, R. Rihm, J. Ganster, H.-P. Fink and M. Sfiligoj Smole (2016). "Tuning of cellulose fibres' structure and surface topography: Influence of swelling and various drying procedures." *Carbohydrate Polymers*, 148, 227-235.

Hult, E.-L., P. T. Larsson and T. Iversen (2002). "A Comparative CP/MAS ^{13}C-NMR Study of the Supermolecular Structure of Polysaccharides in Sulphite and Kraft Pulps." *Holzforschung*, 56(2), 179-184.

Jayme, G. (1958). "Properties of wood celluloses. II. Determination and significance of water-retention value." *Tappi*, 41(11), 180A.

Kabel, M. A., H. van den Borne, J.-P. Vincken, A. G. J. Voragen and H. A. Schols (2007). "Structural differences of xylans affect their interaction with cellulose." *Carbohydrate Polymers*, 69(1), 94-105.

Kadla, J. F. and R. D. Gilbert (2000). "Cellulose structure: A review." *Cellulose Chemistry and Technology*, 34(3-4), 197-216.

Kerssemakers, A. A. J., P. Domenech, M. Cassano, C. K. Yamakawa, G. Dragone and S. I. Mussatto (2020). "Production of Itaconic Acid from Cellulose Pulp: Feedstock Feasibility and Process Strategies for an Efficient Microbial Performance." *Energies*, 13(7), 12.

Kiessling, L. L. and R. C. Diehl (2021). "CH−π Interactions in Glycan Recognition." *ACS Chemical Biology*, 16(10), 1884-1893.

Kron, L., C. Marion de Godoy, M. Hasani and H. Theliander (2023). "Kraft cooking of birch wood chips: differences between the dissolved organic material in pore and bulk liquor." *Holzforschung*, 77(8), 598-609.

Köhnke, T. (2010). *Adsorption of xylans on cellulosic fibres -Influence of xylan composition on adsorption characteristics and kraft pulp properties*. Docotral Thesis, Chalmers University of Technology.

Larsson, P.T., Hult, E.-L., Wickholm, K., Pettersson, E. and Iversen, T. (1999) 'CP/MAS ^{13}C-NMR spectroscopy applied to structure and interaction studies on cellulose I', *Solid State Nuclear Magnetic Resonance*, 15(1), 31–40.

Larsson, P. T., K. Wickholm and T. Iversen (1997). "A CP/MAS ^{13}C NMR investigation of molecular ordering in celluloses." *Carbohydrate Research*, 302(1), 19-25.

Lindgren, J., L.-O. Öhman, S. Gunnars and L. Wågberg (2002). "Charge determinations of cellulose fibres of different origin – Comparison between different methods." *Nordic Pulp & Paper Research Journal*, 17(1), 89-96.

Malmgren, K. and T. Nordqvist (2023). *Production of modified pulp*. U. S. Patent 11,739,477 B2, SCA Forest Products AB (Sundsvall).

Matsuoka, K. (2023). "In Japan, cellulosic nanofibers look to leave the lab." Volume 101, Issue 12. From: https://cen.acs.org/materials/nanomaterials/Japan-cellulosic-nanofibers-look-leave/101/i12. Retrieved 2025-05-03.

Matveev, D., V. Vasilevsky, V. Volkov, T. Plisko, A. Shustikov, A. Volkov and A. Bildyukevich (2022). "Fabrication of ultrafiltration membranes from non-toxic solvent dimethylsulfoxide: Benchmarking of commercially available acrylonitrile co-polymers." *Journal of Environmental Chemical Engineering*, 10(1).

Michell, A. J. (1988). "Second derivative FTIR spectra of celluloses I and II and related mono- and oligo-saccharides." *Carbohydrate Research*, 173(2), 185-195.

Mostafa, T. B., H. F. Naguib, M. W. Sabaa and S. M. Mokhtar (2005). "Graft copolymerization onto chitin and its of itaconic acid properties." *Polymer International*, 54(1), 221-225.

Nippo Paper Group, (2025). "*Cellulose nanofiber manufacturing technology and application development*. From: https://www.nipponpapergroup.com/english/research/organize/cnf.html. Retrieved 2025-05-03.

Nishiyama, Y., J. Sugiyama, H. Chanzy and P. Langan (2003). "Crystal Structure and Hydrogen Bonding System in Cellulose Iα from Synchrotron X-ray and Neutron Fiber Diffraction." *Journal of the American Chemical Society*, 125(47), 14300-14306.

Nouryon. (2025). "CMC Sodium Carboxymethyl Cellulose." From: https://www.nouryon.com/products/cellulose-ethers/cmc/. Retrieved 2025-05-09.

O'Sullivan, A. C. (1997). "Cellulose: the structure slowly unravels." *Cellulose*, 4(3), 173-207.

Paajanen, A., A. Zitting, L. Rautkari, J. A. Ketoja and P. A. Penttilä (2022). "Nanoscale Mechanism of Moisture-Induced Swelling in Wood Microfibril Bundles." *Nano Letters*, 22(13), 5143-5150.

Parton, T. G., R. M. Parker, G. T. van de Kerkhof, A. Narkevicius, J. S. Haataja, B. Frka-Petesic and S. Vignolini (2022). "Chiral self-assembly of cellulose nanocrystals is driven by crystallite bundles." *Nature Communications*, 13(1), 2657.

Patterson, A. L. (1939). "The Scherrer Formula for X-Ray Particle Size Determination." *Physical Review*, 56(10), 978-982.

Pavia, D. L., G. M. Lapman, G. S. Kriz and J. R. Vyvyan (2015). *Infrared spectroscopy. Introduction to Spectroscopy*, Fifth Edition. Stamford, USA, Cengage Learning, p. 14-106.

Revol, J.-F., D. L. Godbout and D. G. Gray (1994). *Solidified liquid crystals of cellulose with optically variable properties*. US5629055A. U.S, FPInnovations.

Revol, J.-F., L. J. Godbout and D. G. Gray (1998). “Solid self-assembled films of cellulose with chiral nematic order and optically variable properties”. *Journal of Pulp and Paper Science*, 24(5), 146-149.

Revol, J. F., H. Bradford, J. Giasson, R. H. Marchessault and D. G. Gray (1992). "Helicoidal self-ordering of cellulose microfibrils in aqueous suspension." *International Journal of Biological Macromolecules*, 14(3), 170-172.

Salmén, L. and J. S. Stevanic (2018). "Effect of drying conditions on cellulose microfibril aggregation and “hornification”." *Cellulose*, 25(11), 6333-6344.

Scherrer, P. (1918). "Bestimmung der Größe und der inneren Struktur von Kolloidteilchen mittels Röntgenstrahlen." Nachrichten von der Gesellschaft der Wissenschaften zu Göttingen, Mathematisch-Physikalische Klasse 1918.

Sirvio, J. A., A. M. Kantola, S. Komulainen and S. Filonenko (2021). "Aqueous Modification of Chitosan with Itaconic Acid to Produce Strong Oxygen Barrier Film." *Biomacromolecules*, 22(5), 2119-2128.

Sjölund, J., G. Westman, L. Wågberg and P. A. Larsson (2025). "High-consistency modification of cellulose fibers: Resource-efficient introduction of cationic charges, and their effect on fiber and nanofibril properties." *Carbohydrate Polymers*, 352, 123254.

Sjöstedt, A., J. Wohlert, P. T. Larsson and L. Wågberg (2015). "Structural changes during swelling of highly charged cellulose fibres." *Cellulose*, 22(5), 2943-2953.

Soto, D., J. Urdaneta, K. Pernia, O. Leon, A. Munoz-Bonilla and M. Fernandez-Garcia (2016). "Itaconic Acid Grafted Starch Hydrogels as Metal Remover: Capacity, Selectivity and Adsorption Kinetics." *Journal of Polymers and the Environment*, 24(4), 343-355.

Spinu, M., N. Dos Santos, N. Le Moigne and P. Navard (2011). "How does the never-dried state influence the swelling and dissolution of cellulose fibres in aqueous solvent?" *Cellulose*, 18(2), 247-256.

Stawski, D. and S. Polowinski (2005). "Polymerization of itaconic acid." *Polimery*, 50(2), 118-122.

Stone, J. E. and A. M. Scallan (1968). "A structural model for the cell wall of water-swollen wood pulp fibres based on their accessibility to macromolecules." *Cellulose Chemistry and Technology*, 2, 343-358.

Tanpichai, S., A. Boonmahitthisud, N. Soykeabkaew and L. Ongthip (2022). "Review of the recent developments in all-cellulose nanocomposites: Properties and applications." *Carbohydrate Polymers*, 286.

Teleky, B.-E. and D. C. Vodnar (2019) "Biomass-Derived Production of Itaconic Acid as a Building Block in Specialty Polymers." *Polymers*, 11(6), 1035.

Virtanen, T., S. Liisa Maunu, T. Tamminen, B. Hortling and T. Liitiä (2008). "Changes in fiber ultrastructure during various kraft pulping conditions evaluated by ^{13}C CPMAS NMR spectroscopy." *Carbohydrate Polymers*, 73(1), 156-163.

Wang, C., C. Tang, Y. Wang, Y. Shen, W. Qi, T. Zhang, R. Su and Z. He (2022). "Chiral photonic materials self-assembled by cellulose nanocrystals." *Current Opinion in Solid State and Materials Science*, 26(5), 101017.

Werpy, T. and G. Petersen (2004). *Top Value Added Chemicals from Biomass: Volume I - Results of Screening for Potential Candidates from Sugars and Synthesis Gas*. United States Department of Energy.

Wickholm, K., P. T. Larsson and T. Iversen (1998). "Assignment of non-crystalline forms in cellulose I by CP/MAS 13C NMR spectroscopy." *Carbohydrate Research*, 312(3), 123-129.

Winter, L., L. Wågberg, L. Ödberg and T. Lindström (1986). "Polyelectrolytes adsorbed on the surface of cellulosic materials." *Journal of Colloid and Interface Science*, 111(2), 537-543.

Wohlert, M., T. Benselfelt, L. Wågberg, I. Furó, L. A. Berglund and J. Wohlert (2022). "Cellulose and the role of hydrogen bonds: not in charge of everything." *Cellulose*, 29(1), 1-23.

Wojno, S. (2023). *Exploring the nonlinear rheological behavior and optical properties of cellulose nanocrystal suspensions*. Doctoral Thesis, Chalmers University of Technology.

Wojno, S., A. K. Sonker, M. Garg, S. Cooper, M. Rigdahl, M. Linares, I. Zozoulenko, R. Kádár and G. Westman (2024). "Cellulose nanocrystal dispersions conjugated with symmetric and asymmetric dialkylamine groups." *Cellulose*, 31(11), 6705-6718.

Zheng, D., J. Zhu, H. Sun, Z. Yu, X. Sun, Y. Zhu, P. Zhu, Y. Ye, Y. Zhang and F. Jiang (2025). "Effect of moisture content on the maleic anhydride mediated disintegration of Kraft pulp into cellulose nanofibrils." *Chemical Engineering Journal*, 509, 161404.

Åhl, A., M.-X. Ruiz-Caldas, E. Nocerino, A. L. C. Conceição, K. Nygård, S. McDonald, M. Viljanen, A. P. Mathew and L. Bergström (2025). "Multimodal structural humidity-response of cellulose nanofibril foams derived from wood and upcycled cotton textiles." *Carbohydrate Polymers*, 357, 123485.